

NASA TECHNICAL NOTE

NASA TN D-4563



NASA TN D-4563

c. 1

LOAN COPY: R
AFWL IW
KIRTLAND ALL

0131125



**CALCULATION OF AXISYMMETRIC
SUPERSONIC FLOW PAST BLUNT BODIES
WITH SONIC CORNERS, INCLUDING A
PROGRAM DESCRIPTION AND LISTING**

*by Jerry C. South, Jr.
Langley Research Center
Langley Station, Hampton, Va.*





CALCULATION OF AXISYMMETRIC SUPERSONIC FLOW PAST
BLUNT BODIES WITH SONIC CORNERS, INCLUDING
A PROGRAM DESCRIPTION AND LISTING

By Jerry C. South, Jr.

Langley Research Center
Langley Station, Hampton, Va.

NATIONAL AERONAUTICS AND SPACE ADMINISTRATION

CALCULATION OF AXISYMMETRIC SUPERSONIC FLOW PAST
BLUNT BODIES WITH SONIC CORNERS, INCLUDING
A PROGRAM DESCRIPTION AND LISTING

By Jerry C. South, Jr.
Langley Research Center

SUMMARY

A program for the approximate calculation of supersonic flow of an ideal gas past blunt bodies with sonic corners is described. Numerical solutions are obtained for the system of differential equations derived from the one-strip integral (Belotserkovskii) method. Aerodynamic results of interest include the surface pressure and velocity distributions, the shape and location of the detached bow shock wave, and the forebody pressure drag coefficient. Comparison of the calculations with experimental data is given, with particular emphasis on spherically blunted cones of large apex angle. For this configuration, a simple method is suggested for estimating angle-of-attack pressure distributions. Other shapes included are a circular disk and a spherical cap convex or concave to the stream. The program operation and listing in FORTRAN IV language are given in the appendixes.

INTRODUCTION

The use of aerodynamic means for deceleration of a body entering a rarified planetary atmosphere such as that of Mars brings high-drag configurations into consideration. In this regard, a blunt body with subsonic flow over most of its "face" is suggested; shapes such as a disk, spherical cap (concave or convex to the stream), and blunted cone with large apex angle thus assume practical importance. Under appropriate conditions, these particular shapes have a common feature: the transition from subsonic to supersonic flow occurs in a singular manner at the sharp, convex corner which terminates the "face." Newtonian aerodynamic analyses do not account for the rapid pressure drop near the sonic corner, so other approximate methods are sought. "Inverse" methods, where the shape of the bow shock wave is given and the body shape is solved for (refs. 1 to 3), are avoided since they can produce only analytic body shapes, whereas the shapes already mentioned have a singularity (corner). Among the "direct" methods (body shape given), one which is particularly adaptable to this problem is the method of integral relations, often called Belotserkovskii's method (refs. 4 to 7). In references 6 and 7, this scheme

was specially developed for use in the first (one-strip) approximation with application to blunt bodies with sonic corners.

Since there is presently a need for more information concerning the nonanalytic, high-drag shapes, this paper presents further results following the method of references 6 and 7, with primary emphasis on spherically blunted cones. The computational program is restricted to an ideal gas (constant specific-heat ratio) and to the singular sonic-point transition; this latter restriction is primarily a geometrical one. A rough, but general, requirement for the occurrence of the singular sonic transition at the corner is that the surface inclination should be everywhere greater than that at the regular sonic point of a full hemisphere. For example, the corner of the convex spherical cap or the junction of the sphere-cone must lie upstream from the usual sonic-point location for the full hemisphere. For any general convex shape with a corner, there is obviously a critical combination of free-stream conditions and minimum surface angle where a smooth-transition sonic point will occur somewhere ahead of the corner. Difficulties are thus encountered when conditions are very near the critical combination, as will be discussed later.

Details of the program symbols, operation, and listing in FORTRAN IV language are given in appendixes A to C.

SYMBOLS

Flow variables are nondimensionalized as follows: pressure by $\rho_\infty V_\infty^2$, density by ρ_∞ , and velocity by V_∞ .

a	local speed of sound
C_D	drag coefficient
D	maximum body diameter
K	body surface curvature, $-d\theta/ds$
M	Mach number, V/a
p	pressure
p_{\max}	stagnation pressure behind normal shock wave
R_b	base radius

R_n	nose radius
s, n	curvilinear coordinates along and normal to body surface (fig. 1)
s_I	value of s at sphere-cone junction
x, r	cylindrical coordinates (fig. 1)
u, v	velocity component in s and n direction, respectively
V	total speed, $\sqrt{u^2 + v^2}$
α	angle of attack
β	shock angle (fig. 1)
γ	ratio of specific heats
δ	shock-layer thickness along n -coordinate (fig. 1)
Φ	stagnation streamline isentrope constant, $p_1(0) / [\bar{p}_1(0)]^\gamma$
$\lambda = \beta - \theta$	
θ	surface inclination angle (fig. 1)
θ_c	cone apex half-angle
$\theta_{c,det}$	apex half-angle of pointed cone at shock detachment
$\theta_{c,son}$	apex half-angle of pointed cone with sonic surface speed
η	fraction of sonic speed for lower bound of surface velocity extrapolation bracket (eq. (7a))
ρ	density
τ	combined entropy-continuity flow variable, $(p/\rho\Phi)^{1/(\gamma-1)}$

Subscripts:

- 0 quantity along surface ($n = 0$)
 1 quantity along shock wave ($n = \delta$)
 ∞ free-stream conditions

Superscript:

- * conditions where $M_0 = 1$

METHOD

Although the basic features of application of the integral method to blunt bodies with sonic corners have been reported before (refs. 6 and 7), there are certain minor variations in procedure which can lead to differences in the numerical results (ref. 8). For the sake of completeness, then, a brief outline is given here.

After the governing partial differential equations (in conservation form as presented in ref. 5) are integrated across the shock layer by approximating certain integrands as linear in n/δ , three ordinary differential equations are obtained, as follows:

$$\frac{d\delta}{ds} = (1 + K\delta)\tan \lambda \quad (1)$$

$$\begin{aligned} \frac{d\beta}{ds} = & \left[(1 + K\delta) \left(\tan \lambda - \frac{\delta \sin \theta}{r_0} \right) \rho_1 u_1 v_1 - (2 + K\delta) \frac{r_1}{r_0} \rho_1 v_1^2 + K\delta \rho_0 u_0^2 \right. \\ & \left. + \left(1 + K\delta + \frac{r_1}{r_0} \right) (p_0 - p_1) \right] \left(\delta \frac{r_1}{r_0} \frac{\partial \rho_1 u_1 v_1}{\partial \beta} \right)^{-1} \end{aligned} \quad (2)$$

$$\begin{aligned} \frac{du_0}{ds} = & \left\{ \left(\tau_1 u_1 - \tau_0 u_0 \right) \frac{d\delta}{ds} - \frac{\delta \sin \theta}{r_0} \left[\tau_0 u_0 + (1 + K\delta) \tau_1 u_1 \right] \right. \\ & \left. - \frac{r_1}{r_0} \left[\delta \frac{\partial}{\partial \beta} (\tau_1 u_1) \frac{d\beta}{ds} + (2 + K\delta) \tau_1 v_1 \right] \right\} \left[\delta \tau_0 (1 - M_0^2) \right]^{-1} \end{aligned} \quad (3)$$

A sketch of the geometry and coordinates is shown in figure 1. A particular body contour is specified by giving the surface angle and curvature, θ and K , as functions of s . The functions at the shock wave are explicit functions of γ , M_∞ , β , and θ . The main dependent variables are δ , β , and u_0 , while p_0 and ρ_0 are obtained as explicit functions of γ , M_∞ , and u_0 by using the isentropic law.

The following notes are offered concerning the derivation of equations (1) to (3):

1. The body-oriented, curvilinear coordinates s, n were used because of their adaptability to a large class of smooth contours (continuous slope up to the sonic corner) and, in particular, to the approach to the singular sonic corner.
2. The "entropy-continuity" formulation, so-called by Xerikos and Anderson (ref. 8), was used instead of the alternate "pure-continuity" formulation because the former gives somewhat better results than the latter in the first approximation.
3. When integrands such as the function $\tau u r$ were approximated by linear interpolation in n/δ between the values at the shock wave and surface, the entire function, including the geometric variable r , was assumed linear in n/δ .

Boundary Conditions and Solution Procedure

At the symmetry axis, $s = 0$, the body surface is normal to the stream ($\theta(0) = \pi/2$), and the following symmetry conditions hold:

$$\beta(0) = \pi/2 \tag{4}$$

$$u_0(0) = 0 \tag{5}$$

At the corner of the body, the surface speed is required to reach sonic value,

$$u_0(s^*) = a^* \tag{6}$$

where a^* is the critical speed, a constant which depends on γ and M_∞ . The integration of equations (1) to (3) starts at $s = 0$ and terminates at $s = s^*$; the initial shock-wave standoff distance $\delta(0)$ is unknown and must be chosen so that equation (6) is satisfied at the correct corner location.

Singularity at the corner.- Inspection of equation (3) shows that the velocity gradient will become infinite at $s = s^*$, since at that point the factor $1 - M_0^2$ vanishes in the denominator, while the numerator does not vanish in general (with exceptions as noted later). In fact, as observed in reference 6, the system of equations (1) to (3) behaves such that the surface speed has a half-power type of singularity in a neighborhood of s^*

$$a^* - u_0 \sim \text{const.}(s^* - s)^{1/2} \quad (7)$$

while β and δ are smooth (continuous s -derivative) functions at s^* . An extrapolation procedure incorporating this feature is used in the numerical calculations when the velocity reaches a value

$$\eta a^* \leq u_0 \leq 0.999a^* \quad (7a)$$

(A value of η which appears to give consistent results is $\eta = 0.95$.)

Determination of $\delta(0)$.- As mentioned before, the initial value of the shock-wave standoff distance $\delta(0)$ is unknown and must be chosen so that the singular sonic point occurs at the known location of the corner. Between successively improved upper and lower bounds, a halving-mode iteration procedure for determining the correct value of $\delta(0)$ is easily automated; for if $\delta(0)$ is too large or too small (within certain limits), the sonic singularity occurs downstream or upstream from the corner, respectively. This behavior is not guaranteed when the desired integral curve lies near the saddle point of the system of equations (1) to (3), mentioned in the next paragraph. Values of $\delta(0)$ which are too large can yield solutions of the other family which have a behavior totally different from that indicated by equation (7) (the numerator of eq. (3) passes through zero before sonic speed is reached). However, such occurrences are easily accounted for in an automatic program. (See also the section entitled "Limitations of Program" for a discussion of sensitivity near the saddle point.)

It should be pointed out that the solution of the blunt-body problem by the one-strip integral approximation is technically easier for the singular sonic-point condition than for the regular sonic-point condition associated with smooth shapes without corners. In the latter case, the sonic point is a saddle point of equations (1) to (3) whose location is not known a priori (ref. 4); the desired solution is the integral curve which passes through the saddle point and divides two divergent families of integral curves. The inherent instability of the saddle-point solution makes its numerical construction difficult, and great accuracy in the initial value $\delta(0)$ is required as a rule (ref. 9). On the contrary, the singular sonic-point solutions are of one family, characterized in behavior by equation (7); in most cases of practical aerodynamic interest, the desired solution is not too near the saddle point, and the relation between $\delta(0)$ and s^* is nearly linear. (In fact, for the circular disk, the relation is exactly linear (ref. 9).) Furthermore, since the sonic corner lies at the maximum body radius, much of the useful information is complete without carrying the solution beyond the corner.

Remarks on Higher Approximations

Higher approximations for the present scheme require the introduction of more strips between the shock wave and body surface. The regular sonic-point condition applies on each intermediate strip boundary, and thus the saddle points appear with a corresponding number of unknown initial parameters. Further technical complications will arise in this scheme if a portion of the subsonic flow, and hence the locus of saddle points, lies beyond the surface normal drawn from the body corner. In this case, polar coordinates might be introduced at the singular corner to complete the determination of the solution, but it is not known if such an approach would be successful or worthwhile. The difficulties associated with the higher approximations certainly justify attempts at obtaining as much useful information as possible from the relatively simple one-strip approximation.

Before these remarks are closed, it should be mentioned that Belotserkovskii has reported some calculations for spherical caps (ref. 10), wherein he combined the two-strip approximation of the so-called scheme II of the integral method (polynomial approximation and explicit integration along the body, numerical integration from the shock wave towards the surface) with Vaglio-Laurin's asymptotic solution for the flow near the sonic corner (ref. 11).

RESULTS AND DISCUSSION

The program as listed in appendix C has a built-in capability to treat four basic axisymmetric "truncated" shapes: a disk normal to the stream, a spherical cap convex or concave to the stream, and a spherically blunted cone. The program can be modified to include other shapes if desired. (See appendix B.) In this section some typical results for these shapes are compared with experimental data, followed by selected results of an exploratory nature for the spherically blunted cone.

Comparison With Experimental Data

An indication of the accuracy and capability of the method can be obtained by comparison with experimental data. The experimental data for the blunted and pointed cones were obtained in the Langley Unitary Plan wind tunnel (UPWT). The pressure data for both blunted and pointed cones and the shock-wave shapes for the blunted cones were supplied by Robert L. Stallings, Jr., Lana M. Couch, and Dorothy H. Tudor; the drag measurements and the shock-wave shapes for the pointed cones were supplied by James F. Campbell. These data are identified in the figures as UPWT data.

Disk and spherical caps (convex to the stream).- Shown in figure 2 are the calculated and measured (ref. 12) pressure distributions for a circular disk and two different

spherical caps (convex to the stream) for $M_\infty = 4.63$. The calculated pressures are consistently too low as the sonic corner is approached, but the accuracy is adequate for engineering design purposes.

Spherical cap concave to the stream. - In figure 3, the calculated pressures for a spherical cap concave to the stream are compared with those of reference 13 for $M_\infty = 4.76$. There is some doubt as to the plotting accuracy of the experimental data since it was replotted from a small-scale figure with a coarse grid (model A in fig. 6 of ref. 13).

Blunt 60° cone. - The calculated and measured results for the bow shock and pressure distribution for a spherically blunted, 60° half-angle cone are shown in figure 4 for $M_\infty = 2.96$ and 4.63, with a bluntness ratio $R_n/R_b = 0.25$. Here also the pressures near the corner are too low by, at most, 3 percent; but again, this accuracy should satisfy engineering requirements. The predicted shape and location of the bow shock wave is seen to be excellent.

Pointed cone with detached shock. - For $\gamma = 1.4$, the bow shock is always detached at any value of M_∞ for a 60° half-angle pointed cone. Hence, when $\theta_c = 60^\circ$ the limit $R_n/R_b \rightarrow 0$ presents no alteration of the important boundary conditions, and it may be expected that the gross features of the solutions for small values of R_n/R_b approach the solution for the pointed cone.¹ Figures 5 and 6 illustrate this feature, showing the calculated results for the bow shock and pressure distribution for $\theta_c = 60^\circ$ and $R_n/R_b = 0.02$ compared with experimental data for a pointed 60° cone. It can be seen that, at least when $\theta_c > \theta_{c,det}$, the calculations for small bluntness ratios are good approximations to the experimental results for both the shock shape and pressures.

On the contrary, when $\theta_c \leq \theta_{c,det}$, the limit $R_n/R_b \rightarrow 0$ does involve discontinuous alteration of an important boundary condition; that is, a pointed cone ($R_n/R_b = 0$) has an oblique shock wave attached at the vertex, and hence the surface entropy is less than that corresponding to the detached, normal shock conditions which hold for any finite blunting ($R_n/R_b > 0$). Even for a pointed cone, the passage from an attached oblique shock to a detached normal shock at $\theta_c = \theta_{c,det}$ implies a discontinuous jump in the surface entropy, and hence a corresponding jump in both the vertex and sonic corner pressures. In spite of this, it seems that the drag of a pointed, finite cone is a continuous function of the cone angle while passing through $\theta_c = \theta_{c,det}$. Busemann (ref. 14) argued

¹Some local nonuniform behavior is anticipated near the stagnation point as $R_n/R_b \rightarrow 0$, since the apex of the pointed cone (with detached shock) is a singular point. The behavior of the flow near the apex is analogous to that of a wedge in incompressible potential flow, where fluid properties vary like s^ν , $0 < \nu < 1$, and ν depends on the apex angle.

that the drag of a sharp wedge depends continuously on the wedge angle through detachment, basing his conclusions on Guderley's potential-flow hodograph analysis (ref. 15). Johnston's (ref. 16) experimental results for both the wedge and cone drag at $M_\infty = 2.45$ appear to be continuous through detachment. His investigation showed that the forebody pressure drag coefficient for a pointed finite cone coincides with that for the infinite cone when $\theta_c \leq \theta_{c,son}$, departs from the infinite-cone value for $\theta_c > \theta_{c,son}$, and increases monotonically and continuously through detachment up to $\theta_c = 90^\circ$. This offers a heuristic picture, then, of the dependence of C_D on θ_c for a pointed finite cone. It remains to consider the effects of small, but finite, bluntness.

A rigorous discussion of the interaction between small blunting and the transonic singularities that arise in the pointed case for $\theta_{c,son} < \theta_c < \theta_{c,det}$ (ref. 15) is beyond the scope of the present report and certainly beyond the means of the coarse one-strip integral method. It seems natural to suppose, however, that the bluntness effects will be contained in an entropy layer whose thickness depends on R_n/R_b and that in the range $\theta_{c,son} < \theta_c < \theta_{c,det}$ the drag coefficient for sufficiently small bluntness will be slightly smaller than that for a pointed cone. The expected difference should be caused by the lower pressure level near the sonic corner of the blunted cone, but the difference in drag should tend to zero as $R_n/R_b \rightarrow 0$ and the bluntness-entropy effects vanish.

The one-strip integral method does not account for vanishingly thin entropy layers; it "weights" the surface entropy condition more or less equally with the shock conditions. Thus as $R_n/R_b \rightarrow 0$, spurious entropy effects remain. Evidence of this can be seen in figure 7, a plot of C_D against θ_c for a finite cone. The experimental data (Campbell, UPWT) were obtained for pointed cones by force measurement and subtraction of the estimated base drag. (The C_D values for $\theta_c = 50^\circ$ were obtained in an earlier test, and were judged to be relatively higher than the others due to a different base drag correction.) The curve corresponding to the infinite-cone solution (showing both the "strong" and "weak" shock branches) was obtained by calculation from the approximate algebraic equations derived from the one-strip integral method by setting the right-hand sides of equations (2) and (3) equal to zero (ref. 17). The calculated curve for the finite "pointed" cone solution is actually for $R_n/R_b = 0.1$. It was found that essentially the same curve is obtained for all values of R_n/R_b from 0.01 to 0.5. (See the next section and fig. 8 concerning the effect of bluntness on drag.) It is clear that the present calculations do not approach the curve for the infinite cone at $\theta_c = \theta_{c,son}$. The gap between the two solutions widens as M_∞ increases, which is in accordance with the increasing difference in the attached- and detached-shock entropy levels at the surface.

Selected Results for the Blunted Cone

Among the shapes considered herein, the spherically blunted cone is by far the most versatile candidate for the aeroshell design of a planetary probe. Both the bluntness ratio and the cone angle can be varied to achieve a compromise among the requirements of convective and radiative heating, drag for deceleration, aerodynamic stability, volume, and so forth. In this section selected results for the blunted cone are presented to indicate some effects of the parameters R_n/R_b , θ_c , γ , and M_∞ .

Insensitivity of drag with bluntness ratio R_n/R_b .- One unexpected result was that the drag remains practically constant as the bluntness ratio is changed from a nearly pointed cone ($R_n/R_b \lesssim 0.1$) to a spherical cap ($R_n/R_b = \sec \theta_c$). In figure 8 this behavior is shown for $\gamma = 1.4$, $\theta_c = 60^\circ$, and $M_\infty = 3, 5, \text{ and } 10$. It is seen that for $0 < R_n/R_b < 1.5$, the change in drag is not measurable, and the drag of the spherical cap ($R_n/R_b = 2.0$) is only 3 percent greater than the pointed-cone drag. On the other hand, the simple Newtonian approximation for the sphere-cone drag coefficient is

$$C_D = 2 \sin^2 \theta_c + \left(R_n/R_b \right)^2 \cos^4 \theta_c \quad (8)$$

which predicts a 17-percent increase in passing from the pointed cone to the spherical cap (for $\theta_c = 60^\circ$). Pressure distributions for several bluntness ratios are shown in figure 9 for the 60° sphere-cone, and it is seen that the smaller bluntness ratios result in slightly higher pressures on the outboard conical skirt where the area contribution is the greatest. This compensating feature is not accounted for in the Newtonian theory; hence, the approximation of equation (8) significantly overestimates the effect of bluntness on drag for the sphere-cone.

Bluntness effect on shock standoff distance and velocity gradient.- Figures 10 and 11 are presented to show how the bow shock standoff distance $\delta(0)/R_b$ and the stagnation-point velocity gradient du_0/ds depend on the bluntness ratio for $\theta_c = 60^\circ$ and $M_\infty = 3, 5, 10, \text{ and } 1000$. Over the entire range of bluntness ratios from the pointed cone to the spherical cap, $\delta(0)/R_b$ is practically a linear function of R_n/R_b . On the contrary, the behavior of the velocity gradient is quite nonlinear. As $R_n/R_b \rightarrow 0$, the combination $R_n du_0/ds$ approaches a finite positive limit, while $R_b du_0/ds$ becomes infinite, like $(R_n/R_b)^{-1}$. But even the qualities of the behavior near $R_n/R_b = 0$ should be regarded with suspicion, for, as mentioned earlier, the velocity behaves in a precise singular manner at the tip of a pointed cone; this is not accounted for in these calculations with a finite (even though small) nose radius.

It should also be noted, according to reference 18, that the velocity gradient predicted by the one-strip integral method for a smooth body (without a sonic corner) is

apparently too large. There is no reason to assume that the present results are more accurate.

Effect of γ on shock shape and pressure distribution.- For a given value of M_∞ , the density ratio across the bow shock increases with decreasing γ , while the calculated shock wave moves closer to the body. Since large density ratios and thin shock layers are characteristic of hypersonic real-gas flows, ideal-gas calculations for low values of $\gamma(\gamma \rightarrow 1)$ are sometimes used to simulate real-gas effects (ref. 1) - at least in regard to the shock shape and surface pressures. The shock-wave shape and pressure distribution for $M_\infty = 10$, $\theta_c = 60^\circ$, and $R_n/R_b = 0.25$ are shown for several values of γ in figures 12 and 13. Values of γ lower than 1.18 cannot be considered for this combination of M_∞ , θ_c , and R_n/R_b , because of the proximity to the condition where the sonic point of the full hemisphere would occur at the sphere-cone junction. (See section "Limitations of Program.") The outstanding feature of these curves is the changing character of the solution as conditions are approached which are appropriate to attached-shock, fully supersonic flow for a pointed cone. For $M_\infty = 10$ and $\theta_c = 60^\circ$, a pointed cone will have an attached shock and supersonic flow at the surface for $\gamma < 1.27$ (fig. 21). It is significant that for $\gamma = 1.27$ two inflection points ($d\beta/ds = 0$) appear on the shock wave of the blunted cone beyond the sphere-cone junction (fig. 12). In figure 13 it can be seen that the pressures have a small relative minimum just ahead of the sphere-cone junction for $\gamma < 1.27$, followed by a large recompression beyond the junction. For reference purposes, the locations of the shock-wave inflection points are indicated on each corresponding pressure curve.

Traugott (ref. 19), among others, has discussed the connection between the appearance of shock-wave inflections and surface-pressure recompressions in flows over blunted cones. In that study, however, the flow at the surface in the recompression region was already supersonic, and the outgoing compression characteristics reached the shock wave (and caused inflections) somewhat downstream. Here the surface flow is subsonic, and the recompression is sensed at the shock almost immediately. For the lowest values of γ , the solution in the nose region approaches that of a complete, smooth sphere, and is practically independent of the afterbody size and shape; while the solution beyond the junction approaches asymptotic ($R_n/R_b \rightarrow 0$) conical pressure and shock angle before the expansion at the sonic corner begins to take effect.

Effect of θ_c on shock and pressure distribution.- For fixed values of γ and M_∞ the pointed sonic cone condition can also be attained by decreasing θ_c . For $\gamma = 1.4$, $M_\infty = 10$, the sonic angle for a pointed cone is $\theta_{c,son} = 54.6^\circ$. Figures 14 and 15 show that the effects of decreasing θ_c for a blunted cone ($R_n/R_b = 0.25$) are qualitatively the same as those already discussed in the previous subsection, where γ was decreased. In figure 14, the body shape was drawn for $\theta_c = 51^\circ$, while only the base corner positions

were indicated for the larger angles. (Note in fig. 15 that the sphere-cone junction locations differ slightly for each value of θ_c .) Figure 16 shows how the shock standoff distance decreases with θ_c , and the independence of the nose solution is clearly evident for $\theta_c < \theta_{c,son} \approx 55^\circ$.

Simple pressure estimates for angle of attack. - It was noted that the pressure distributions for values of θ_c larger or smaller than the nominal value, say $\theta_c = 60^\circ$, bear a strong resemblance to the experimental distributions on the windward and leeward generators of a 60° blunted cone at angle of attack. To investigate the possibilities of making some quantitative estimates, a 60° blunted cone at 5° angle of attack was considered. Pressure data (Stallings, Couch, and Tudor, UPWT) for that configuration at $M_\infty = 4.63$ are shown in figure 17, together with the present results for $\theta_c = 65^\circ$ and 55° , approximating the windward and leeward pressure distributions, respectively. It appears that the levels of the predictions are roughly in accord, but some coordinate shifting and stretching might help to account for (1) the displaced stagnation point and (2) the altered distance to the sonic corner. One quick and obvious scheme is to shift the stagnation point to the most forward point of the nose and cause the sonic corners to occur at the correct location by a linear transformation. That is, the simulated windward ($\theta_c = 65^\circ$) and leeward ($\theta_c = 55^\circ$) pressure calculations are relocated by correcting the corresponding s/D values by a term which depends linearly on s . For this example (60° blunted cone at 5° angle of attack),

$$\begin{aligned} \left(\frac{s}{D}\right)_{\text{wind}} &= -\left(\frac{s}{D}\right)_{65} - \frac{\Delta}{D} - \left[\left(\frac{s^*}{D}\right)_{60} - \left(\frac{s^*}{D}\right)_{65} - \frac{\Delta}{D} \right] \left(\frac{s}{s^*}\right)_{65} \\ &= -\left(\frac{s}{D}\right)_{65} - 0.011 - 0.012 \left(\frac{s}{s^*}\right)_{65} \end{aligned}$$

and

$$\begin{aligned} \left(\frac{s}{D}\right)_{\text{lee}} &= \left(\frac{s}{D}\right)_{55} - \frac{\Delta}{D} - \left[\left(\frac{s^*}{D}\right)_{55} - \left(\frac{s^*}{D}\right)_{60} - \frac{\Delta}{D} \right] \left(\frac{s}{s^*}\right)_{55} \\ &= \left(\frac{s}{D}\right)_{55} - 0.001 - 0.018 \left(\frac{s}{s^*}\right)_{55} \end{aligned}$$

where Δ is the displacement required to shift the stagnation point to the most forward nose point (which lies on the spherical portion for $\alpha \leq 30^\circ$),

$$\frac{\Delta}{D} = \frac{\alpha R_n}{D}$$

The results with the shifted and stretched coordinates are replotted in figure 18, together with similar calculations and data for $\alpha = 10^\circ$. Figure 19 shows the comparison for $M_\infty = 2.96$. The agreement for the leeward pressure distribution is surprisingly accurate, while the windward results agree within 5 percent. This approximation may be particularly useful if it is coupled with some empirical fit for the peripheral pressure distribution such as the second-degree trigonometric polynomial suggested by Kaattari (ref. 20). Hence there exists the capability of obtaining, quite cheaply, reasonable estimates for the entire forebody pressure distribution.

LIMITATIONS OF PROGRAM

Smooth Sphere Sonic Point at Junction

The main difficulty in this program is encountered for the sphere-cone shape when conditions are approached such that the sonic point for a complete, smooth sphere would occur at the sphere-cone junction.² The sonic point for the smooth sphere is a saddle point of the differential equations (1) to (3) (ref. 4), and the diverging integral curves near the saddle point are extremely sensitive to the value of $\delta(0)$. For combinations of γ , M_∞ , and θ_c near this condition, the success or failure of convergence depends on three factors: (1) the number of figures carried in the calculations (i.e., the "word" length of the computer), (2) the bluntness ratio R_n/R_b , and (3) the prescribed accuracy criterion ϵ for placing the sonic singularity $\left(\left| r_0^*/R_b - 1 \right| \leq \epsilon \right)$. An example follows.

Figure 20 is an illustration of the sensitivity of the solution on $\delta(0)$ near the critical condition. For $\gamma = 1.4$ and $M_\infty = 10$ the sonic point for a smooth sphere occurs at a location where the surface angle θ , and hence the critical cone angle θ_c is about 49.1° . But even for $\theta_c = 52^\circ$, eight correct figures in $\delta(0)/R_n$ were required to place the sonic singularity slightly beyond $r_0^*/R_n = 4.0$. In other words, if only eight decimal figures were carried in the calculations, bluntness ratios less than about 0.25 could not be obtained, and those somewhat greater than 0.25 would be possible only for a fairly lax convergence criterion (say $\epsilon \gtrsim 0.05$). For $\theta_c = 51^\circ$, $R_n/R_b = 0.25$, forty-five

²In an exact analysis, the chief concern would be the point of origin of the limiting characteristic (ref. 1, pp. 202-203), downstream from which changes in the body shape cannot affect the nose solution. In the one-strip approximation, however, it is the surface sonic point that is crucial.

halving-mode iterations (producing about fourteen correct figures³ in $\delta(0)/R_n$) were required for an accuracy criterion $\epsilon = 10^{-4}$.

In a study of blunted cones of "small" angle (i.e., with sonic point always on the spherical nose), Traugott (ref. 19) described a range of cone angles in which the integral method should fail, for a given γ and M_∞ . The upper limit is the critical angle just described; that is, the cone angle θ_c for which the sonic point of the complete smooth sphere would occur at the sphere-cone junction. The lower limit is the cone angle for which the asymptotic, pointed-cone pressure is equal to the sonic pressure obtained by isentropic expansion from the normal shock conditions. The cone angles in between constitute what Traugott called the "second sonic point" region; wherein the flow along the surface will become supersonic on the spherical nose, but must become subsonic again if asymptotic conical pressure is to be reached downstream. While Traugott found the method to fail upon approaching this range of angles from below, the present program fails upon approaching from above.

Unfortunately, there are not available any extensive tabulations of the sonic-point location on a sphere for various combinations of γ and M_∞ . In fact, it is that information for the one-strip integral method that is needed here, for the purpose of avoiding the critical condition when using this program. A more practical limit, which can be charted profusely, is the sonic condition for the pointed cone, $\theta_{c,son}(\gamma, M_\infty)$. It was found that this condition lies fairly close to the "smooth sphere sonic-point" condition and will serve as a guide in warning the program user of expected sensitivity and possible nonconvergence. Figure 21 is a chart of the pointed sonic cone condition; the calculations were performed by using the algebraic equations which approximate conical flow by setting the right-hand sides of equations (2) and (3) equal to zero (ref. 17).

Convex or Concave Spherical Caps

The same difficulties are to be expected for the spherical cap (convex to the stream) when the corner is near the smooth sphere sonic point. For the concave spherical cap, no extensive investigation was undertaken to determine the limits of applicability of the present program. An obvious geometrical condition to be avoided for this shape is the intersection of the surface normals within the shock layer — that is, since

³A reliable estimate for the number of halving-mode iterations N_{hm} required to produce N_d decimal figures in $\delta(0)/R_n$ is

$$N_{hm} \approx N_d / \log_{10} 2 \approx 3.3N_d$$

$K = -d\theta/ds = -1$ for the concave spherical cap, the condition $K\delta \leq 1$ might occur. It is possible that this could happen for low values of M_∞ and/or values of R_n/R_b approaching 1.0 (from above).

M_∞ Too Small

As M_∞ decreases, the shock wave moves farther away from the body and the sonic point on the shock wave moves up, away from the axis. For a given body shape, a value of $M_\infty > 1$ will be reached where a considerable portion of the subsonic flow region lies beyond the normal drawn from the sonic corner of the body. It would seem that such solutions would be either nonexistent or meaningless in the one-strip integral approximation, since the calculation ends when the sonic corner is reached, and hence a part of the subsonic flow would be ignored. Such a situation is, of course, both physically and mathematically objectionable.

What appears to happen in the one-strip approximation, at least in all cases studied so far, is the following: the shock-wave sonic point always occurs ahead of the surface normal drawn from the sonic corner of the body, which implies proper closure of the subsonic region. But since the shock wave has less curvature near the axis as M_∞ decreases, it must turn more rapidly as the sonic corner is approached to achieve the sonic shock angle; the factor $\partial(\rho_1 u_1 v_1)/\partial\beta$ in the denominator of $d\beta/ds$ becomes small near the corner, resulting in the rapid increase in magnitude of $d\beta/ds$. Ultimately a value of M_∞ is reached where $\partial(\rho_1 u_1 v_1)/\partial\beta$ passes through zero at the corner, and hence the shock has infinite curvature there. The disk provides a good example of this difficulty. In table I are given values of $\partial(\rho_1 u_1 v_1)^*/\partial\beta$ as M_∞ decreases from hypersonic values; it is clear that two-fold smooth (continuous curvature) shock-wave solutions do not exist below $M_\infty \approx 2.3$.

TABLE I.- APPROACH TO SHOCK CURVATURE SINGULARITY FOR A DISK

M_∞	$\delta(0)/R_b$	$\partial(\rho_1 u_1 v_1)^*/\partial\beta$
10.0	0.470	2.004
6.0	.494	1.812
4.0	.541	1.464
3.0	.607	.997
2.4	.703	.284
2.3	.732	.024

CONCLUDING REMARKS

The present program has the capability for calculating good approximations to the shock-wave shape and surface pressure distribution for blunt bodies with sonic corners. Typical results for the disk, concave or convex spherical caps, and sphere-cones agree well with experimental data.

The flow past a pointed cone was approximated by calculations for a sphere-cone with small bluntness ratio. It was found that results were generally good for cone angles larger than the detachment angle; but results were not satisfactory as the cone angle was decreased to and below the detachment angle. The reason for this appears to be the inability of the method to account for a vanishingly thin entropy layer.

For the blunted cone, inflection points occur in the shock wave when the sonic condition for a pointed cone is reached. This condition can be reached, for example, by decreasing the cone angle. Further decreases in cone angle cause the nose and afterbody solutions to become nearly independent of each other.

It was found that reasonable estimates could be made for angle-of-attack pressure distributions in the symmetry plane of a blunt cone. The windward and leeward distributions were simulated by adding and subtracting the angle of attack from the cone angle, respectively.

A critical condition for the method is evident in the application to sphere-cones and spherical caps. It occurs when the combination of parameters (cone angle or surface inclination angle at the sonic corner, Mach number, and specific heat ratio) is such that the natural sonic-point location for the complete sphere lies at the sphere-cone junction or the spherical cap corner. Depending on the bluntness ratio, extreme sensitivity and nonconvergence is encountered somewhat before this condition is reached.

For a given body shape, there is a minimum Mach number below which no two-fold smooth (continuous curvature) shock solutions exist. The accuracy of the solutions near this minimum value is questionable, particularly near the sonic corner. For the disk, the minimum Mach number was about 2.3 (in air).

Langley Research Center,
National Aeronautics and Space Administration,
Langley Station, Hampton, Va., February 13, 1968,
129-01-03-06-23.

APPENDIX A

PROGRAM SYMBOLS

The FORTRAN symbols appearing in the input, headings, and output of this program (appendix C) are given in the left-hand column, and their meanings defined in terms of standard notation or the symbols defined in the section "Symbols" are given in the right-hand column. These program symbols are as follows:

Input:

LC	body shape trigger, 1, 2, 3, or 5 for disk, convex spherical cap, blunted cone, or concave spherical cap, respectively
MM	loop counter, number of cases (combinations of γ , M_∞ , θ_c , and R) for a given body shape (LC)
GAMMA	γ
AMINF	M_∞
THETAC	θ_c , cone half-angle in degrees for blunt cone (LC = 3); dummy input value for other shapes (other LC)
R	sonic-point radius parameter, 1.0 for disk (LC = 1) and r_0^*/R_n for other shapes (other LC)

Case heading (other than symbols defined for input):

DELO	$\delta(0)$, initial standoff distance in appropriate length scale (as explained in appendix B)
DS	initial integration step size
ETA	η (see eq. (7a))
SI	value of s at sphere-cone junction (LC = 3); dummy value for other shapes

APPENDIX A

NIS	number of integration steps in final run
NIR	number of integration runs to find correct $\delta(0)$
CD	forebody pressure drag coefficient (referred to base area πr_0^2 for all shapes)

Output (the output is printed across in a block of three rows for each integration step):

S	s
BETAD	β , degrees
THETAD	θ , degrees
XO	x_0
RO	r_0
UO	u_0
PO	p_0
RHOO	ρ_0
TO	temperature ratio, T_0/T_∞
DELTA	δ
X1	x_1
R1	r_1
V1	v_1
U1	u_1
P1	p_1

APPENDIX A

RHO1	ρ_1
DS	integration step size
DBDS	$d\beta/ds$
DUODS	du_0/ds
POBAR	p_0/p_{\max}
SBAR	s/s^*

Main program (some of the more important FORTRAN symbols used in the main program):

DSC	starting step size for each integration run
LN	overall print trigger, 1 for no print and 0 for print (switched to zero when correct $\delta(0)$ is found)
N	step print trigger, 0 for no print and 1 for print (only print when stable step is completed)
L	body shape trigger, equal to LC but switched to 4 for rescaling when $LC = 3$ (see description of body shape subroutine in appendix B)
LL	trigger for double-valued curvature at sphere-cone junction, 1 for sphere curvature and 2 for zero curvature
LLL	step size trigger, 1 until step size is halved to achieve velocity bracket and 2 thereafter (see program statement 54)
LLLL	halving mode trigger, 1 until upper and lower bounds for $\delta(0)$ are found and 2 thereafter

Body shape subroutine:

THETA	θ , radians
AK	K, surface curvature

APPENDIX B

PROGRAM OPERATION

See main text section entitled "Limitations of Program" before operating this program.

General Remarks

The FORTRAN IV program listed in appendix C was originally developed for the IBM 7094 electronic data processing system, and subsequently it was modified for use in the Control Data 6600 computer system. Other than using control cards which are appropriate to an individual system, the changes necessary to operate the program on the IBM 7094 system are as follows:

- (1) Remove the two instructions in statement 1,

```
IF (EOF,5) 9999,1000  
9999 STOP
```

- (2) In statement 2, change the thirteenth instruction to:

```
IF (NIR.LT.31) GO TO 2000
```

The reason for change (2) is the shorter single-precision word length of the IBM system (eight decimal digits). More than 27 halving iterations for $\delta(0)$ will not change the eight decimal digits carried in the calculations. About four runs are allotted for finding upper and lower bounds for $\delta(0)$.

A large number of comment cards were included to highlight the various sections of the program. A fourth-order Runge-Kutta integration scheme was built into the program so that a "library" routine would be unnecessary. Also, a rule-of-thumb step size variation scheme is used which is very simple yet adequate for these calculations. It tests on the shock-angle derivative $d\beta/ds$ and seeks a step size such that the "predicted" and "corrected" values for $d\beta/ds$ at the interval midpoint are within a few percent of each other. Numerical stability and accuracy are not a problem in these calculations.

Initial estimates for DELO.- For each of the four shapes included, the initial estimate for $\delta(0)$ is automatically computed, as follows:

APPENDIX B

LC	Shape	DELO	Source
1	Disk	$1.03/\sqrt{\rho_1(0) - 1}$	Ref. 21
2	Convex sphere cap	$.667/[\rho_1(0) - 1]$	Ref. 21
3	Sphere-cone	$.667R/[\rho_1(0) - 1]$	-----
5	Concave sphere cap	$1.03R/\sqrt{\rho_1(0) - 1}$	-----

Accuracy criterion.- The accuracy criterion for locating the sonic corner is listed as 10^{-4} ; that is, $|\text{ROST}/R - 1| \leq 10^{-4}$ (see the fourth instruction from the end of statement 60). This can be relaxed, if necessary, to achieve convergence closer to the "critical condition" described in the main text in the section "Limitations of Program."

Modifications for other body shapes.- The program can be modified to include other shapes in the body shape subroutine (BSR) by adding more statements, triggers, and, if there are more than two segments to the shape, more junction locations SII, SIII, etc. Care must be taken to insure that an integration step coincides with each junction location, and that the curvature of the segment upstream or downstream from the junction is properly used. Some study of the logic for the sphere-cone shape (LC = 3) should help in this respect; the crucial locations in the main program are the last 'TF(. . .)' instructions in statements 30 and 52.

Some reasonable initial value for DELO must be given for any new body shapes, or otherwise the initial DELO will be estimated for a sphere.

Input

The first four cards (ER, BLK, BCK, ERR) are always necessary to the program, and they provide for specific error messages or debug information.

NNN is the debug trigger. If NNN = 0, debug information is printed out; a dummy fixed-point number different from 0 is read in if no debug information is needed.

LC is the body shape trigger; MM is the number of cases to be run for that value of LC. For each case, one card is required, with values for GAMMA (γ), AMINF (M_∞), THETAC (θ_c), and R.

For LC = 3 (the sphere-cone) THETAC is the cone half-angle in degrees; for other LC, a dummy value must be input.

R is the sonic corner location parameter. For LC = 1 (disk), $R = 1$. For the three other shapes, $R = r_0^*/R_n$. Note that for the sphere-cone, R is the reciprocal of the bluntness ratio $(R_n/R_b)^{-1}$.

APPENDIX B

Case Heading and Output

See appendix A for a description of the symbols in the case heading and output. For each integration step, a three-line block of 21 values is printed.

Length scale.- The appropriate length scale is as follows for the four body shapes:

Disk	$R_b = 1$
Concave or convex sphere cap	$R_n = 1$
Sphere-cone	$R_b = 1$

Sample Cases

At the end of the listing in appendix C, some sample input cards are listed. After the four error- and debug-message cards, the NNN value is 1 (for no debug). Then all four body shapes are run: one case each for the disk (LC = 1) and the concave spherical cap (LC = 5) and two cases each for the convex spherical cap and the sphere-cone. The total central processing unit time for all six cases on the Control Data 6600 computer system was about 18 seconds. The correct value of DELO ($\delta(0)$ to the appropriate length scale as already described) is listed for each case in order in the following table (15 decimal figures carried in calculations):

Shape	LC	MM	GAMMA	AMINF	THETAC	R	DELO
Circular disk	1	1	1.4	4.63	a1.0	1.0	b0.519443847
Spherical cap, convex to stream	2	2	1.4	4.63	a1.0	0.25882	c0.107979173
			1.4	4.63	a1.0	0.5	c0.156923693
Spherically blunted cone	3	2	1.4	4.63	60.0	4.0	b0.0921382953
			1.4	4.63	60.0	50.0	b0.0556326561
Spherical cap, concave to stream	5	1	1.4	4.76	a1.0	0.25882	c0.160711018

^aDummy input.

^b $\delta(0)/R_b$.

^c $\delta(0)/R_n$.

APPENDIX C
PROGRAM LISTING

APPENDIX C

```

C  TRUNCATED BLUNT BODY
   COMMON ER(12),BLK(12),BCK(12),ERR(12),THETA,THETAD,AK,RBETAD,ALAMB
   1,CON1,CON2,CON3,CON4,CON5,CON6,CON7,C90,C91,NNN,U1,V1,P1,GAMMA,RHO
   21,ST1,Z1,H1,R1,X1,CPhi,RH00,PO,AOSQ,STO,PHI,DDDS,DBDS,DUODS,DRODS,
   3DXODS,TO,AOST,BETA,FAC,DENOM,DENOM1,DFDS,CD,R,PU1PB,POBAR,SMAX,
   4SBAR,LN,DELTAL,DELO,DELTAU,NIR,NIS,L,PZ1PB
800 FORMAT(25H DAVIS-DLD-A1054C-3-15-66)
801 FORMAT(12H JERRY SOUTH)
802 FORMAT(21H TRUNCATED BLUNT BODY//)
805 FORMAT(31H CIRCULAR DISK NORMAL TO STREAM//)
806 FORMAT(31H SPHERICAL CAP CONVEX TO STREAM//)
807 FORMAT(43H SPHERICALLY-BLUNTED CONE,CONE HALF-ANGLE =,E16.8//)
808 FORMAT(32H SPHERICAL CAP CONCAVE TO STREAM//)
809 FORMAT(25H ITERATION COUNT EXCEEDED/)
   90 FORMAT(12A6)
   91 FORMAT(10I5)
   92 FORMAT(5E14.8)
   93 FORMAT(1X6HGAMMA=E16.8,2X6HAMINF=E16.8,2X5HDELO=E16.8,2X3HDS=E16.8
   1)
   94 FORMAT(1X1A6/(8E16.8))
   95 FORMAT(1X12A6//)
   96 FORMAT(15H DELO TOO LARGE)
   97 FORMAT(8X1HS14X5HBETAD10X6HTHETAD12X2HX014X2HR014X2HU014X2HP013X4H
   1RH00/7X2HT014X5HDELTA12X2HX114X2HR114X2HV114X2HU114X2HP113X4HRH01/
   27X2HDS14X4HDBDS12X5HDUODS11X5HPOBAR11X4HSBAR//)
   98 FORMAT(//)
   99 FORMAT(1X8E16.8/1X8E16.8/1X5E16.8/)
100 FORMAT(//)
102 FORMAT(1X4HETA=E16.8,2X2HR=E16.8,2X3HSI=E16.8,2X4HNIS=I5,2X4HNIR=I
   15,2X3HCD=E16.8//)
   WRITE(6,800)
   WRITE(6,801)
   WRITE(6,802)
   DEG=57.295780
   PI=3.1415927
   PI2=PI/2.
   READ(5,90)ER,BLK,BCK,ERR
   READ(5,91)NNN
   1 READ(5,91)LC,MM
   IF(EOF,5)9999,1000
9999 STOP
1000 DO 71 MMM=1,MM
   READ(5,92)GAMMA,AMINF,THETAC,R
C  COMPUTATION OF CONSTANTS AND STARTING PARAMETERS
   ETA=.95

```

APPENDIX C

```

SI=.1E+06
IF(LC.EQ.3)SI=(90.-THETAC)/DEG
DSC=.05
IF(LC.EQ.3)DSC=SI/10.
CON3=GAMMA-1.
CON4=GAMMA+1.
CON1=4./CON4
CON2=AMINF**2
CON5=CON3/(2.*GAMMA)
CON6=1./(GAMMA*CON2)
CON7=1./CON3
L=LC
DENS1=2.*(CON2-1.)/(2.+CON3*CON2)
DELO=.667/DENS1
IF(L.EQ.3)DELO=R*DELO
IF(L.EQ.1.OR.L.EQ.5)DELO=1.03*R/SQRT(DENS1)
DELTAL=DELO
NIR=0
LN=1
LLLL=1
C  INITIAL VALUES
  2  LL=1
    LLL=1
    N=0
    DS=DSC
    S=0.0
    CALL BSR(L,LL,SI,S)
    IF(LN.EQ.0.AND.L.EQ.1)WRITE(6,805)
    IF(LN.EQ.0.AND.L.EQ.2)WRITE(6,806)
    IF(LN.EQ.0.AND.LC.EQ.3)WRITE(6,807)THETAC
    IF(LN.EQ.0.AND.L.EQ.5)WRITE(6,808)
    IF(LN.EQ.0)WRITE(6,93)GAMMA,AMINF,DELO,DS
    IF(LN.EQ.0)WRITE(6,102)ETA,R,SI,NIS,NIR,CD
    IF(NIR.LT.50)GO TO 2000
    IF(LN.EQ.0)WRITE(6,809)
    IF(L.EQ.2)THETST=SST*DEG
    IF(LN.EQ.0)WRITE(6,94)ER(1),DELTAL,DELO,DELTAU,SST,ROST,THETST
    IF(LN.EQ.0)STOP
    LN=0
    GO TO 2
2000 NIS=0
    NIR=NIR+1
    IF(LN.EQ.0)WRITE(6,97)
    U0=0.0
    BETA=PI/2

```

APPENDIX C

```

      BETAD=BETA*DEG
      DELTA=DELO
      RO=0.0
      XO=0.0
      F=0.0
200 CALL SHOCK(S,UO,BETA,DELTA,RO,XO,F)
      DISC=-V1
      IF(NNN.EQ.0)WRITE(6,94)BLK(1),ALAMB,B,A,P1,RHO1,V1,DISC,DELTA,BETA
1,UO,RO,XO,THETA,R1,X1,U1
      IF(DISC.LT.0.0.0R.RHO1.LE..00001)GO TO 20
      AOST=SQRT(DISC)
      TEST=ETA*AOST
C INITIAL DERIVATIVES
      IF(NNN.EQ.0)WRITE(6,94)BLK(2),AOST,TEST,CPhi,H1,FAC,RHOO,PO,PU1P
1B,AOSQ,TO
      GO TO 24
20 WRITE(6,94)ER(1),DISC,RHO1
      GO TO 71
24 DENOM=DELTA*H1*PU1PB
      IF(ABS(DENOM).LE..00001)GO TO 26
      DBDS=(PO-P1-V1*H1)/DENOM
      DENOM1=DELTA*RHOO*V1
      IF(ABS(DENOM1).LE..00001)GO TO 27
      DUODS=- (1.+AK*DELTA)*(PO-P1)/DENOM1
      DDDS=0.0
      DRODS=1.0
      DXODS=0.0
      DFDS=0.0
      CD=2.*(PO-CON6)
      HUO=UO
      IF(LN.EQ.0)WRITE(6,99)S,BETAD,THETAD,XO,RO,UO,PO,RHOO,TO,DELTA,X1,
1R1,V1,U1,P1,RHO1,DS,DBDS,DUODS,POBAR,SBAR
25 IF(NNN.EQ.0)WRITE(6,94)BLK(3),DENOM,DBDS,DENOM1,DUODS,DDDS,DRODS,D
1XODS
      GO TO 31
26 WRITE(6,94)ER(4),DENOM
      GO TO 71
27 WRITE(6,94)ER(5),DENOM,DENOM1
      GO TO 71
C RUNGE-KUTTA INTEGRATION (FOURTH ORDER ROUTINE) WITH VARIABLE STEP SIZE
30 IF(L.EQ.2.AND.RS.GE.1.5707)GO TO 71
      CALL BSR(L,LL,SI,RS)
      CALL SHOCK(RS,RUO,RBETA,RDELTA,RRO,RXO,RF)
      IF(L.GT.1.AND.PZ1PB.LT..1)GO TO 530
      IF(LN.EQ.0.AND.N.EQ.1)WRITE(6,99)RS, RBETAD, THETAD, RXO, RRO, RUO, PO,

```

APPENDIX C

```

1RHOO,TO,RDELTA,X1,R1,V1,U1,P1,RH01,DS,DBDS,DUODS,POBAR,SBAR
N=0
IF(SIN(RBETA)**2.LE..00001.OR.ABS(COS(ALAMB)).LE..00001.OR.FAC.LT.
10.0.OR.ABS(RHOO).LE..00001.OR.ABS(RRO).LE..00001.OR.ABS(DENOM).LE.
2.00001.OR.ABS(DENOM1)).LE..00001)GO TO 71
IF(LL.EQ.2)GO TO 31
C CHECK ON LOCATION OF SPHERE-CONE JUNCTION
IF(S+DS.LE.S1)GO TO 31
DS=SI-S
31 A1=DS*DUODS
B1=DS*DBDS
C1=DS*DDDS
D1=DS*DR0DS
E1=DS*DX0DS
F1=DS*DFDS
IF(NNN.EQ.0)WRITE(6,94)BLK(4),A1,B1,C1,D1,E1,F1
RS=S+DS/2.
RUO=UO+A1/2.
IF(RUO.GT..999*AOST)GO TO 54
RBETA=BETA+B1/2.
RDELTA=DELTA+C1/2.
RRO=RO+D1/2.
RXO=XO+E1/2.
RF=F+F1/2.
CALL BSR(L,LL,S1,RS)
CALL SHOCK(RS,RUO,RBETA,RDELTA,RRO,RXO,RF)
IF(SIN(RBETA)**2.LE..00001.OR.ABS(COS(ALAMB)).LE..00001.OR.FAC.LT.
10.0.OR.ABS(RHOO).LE..00001.OR.ABS(RRO).LE..00001.OR.ABS(DENOM).LE.
2.00001.OR.ABS(DENOM1)).LE..00001)GO TO 71
A2=DS*DUODS
B2=DS*DBDS
C2=DS*DDDS
D2=DS*DR0DS
E2=DS*DX0DS
F2=DS*DFDS
IF(NNN.EQ.0)WRITE(6,94)BLK(5),A2,B2,C2,D2,E2,F2
RUO=UO+A2/2.
IF(RUO.GT..999*AOST)GO TO 54
RBETA=BETA+B2/2.
RDELTA=DELTA+C2/2.
RRO=RO+D2/2.
RXO=XO+E2/2.
RF=F+F2/2.
CALL BSR(L,LL,S1,RS)
CALL SHOCK(RS,RUO,RBETA,RDELTA,RRO,RXO,RF)

```

APPENDIX C

```

    IF (SIN(RBETA)**2.LE..00001.OR.ABS(COS(ALAMB)).LE..00001.OR.FAC.LT.
    10.0.OR.ABS(RHOO).LE..00001.OR.ABS(RRO).LE..00001.OR.ABS(DENOM).LE.
    2.00001.OR.ABS(DENOM1).LE..00001)GO TO 71
    A3=DS*DUODS
    B3=DS*DBDS
    IF (ABS(B2).LT..1E-05.OR.LLL.GT.1)GO TO 32
C  INTEGRATION ACCURACY STEP-SIZE TEST
    DSTEST=ABS((B2-B3)/B2)
    IF (DSTEST.LE..05)GO TO 32
    DS=.5*DS
    IF (DS.GT..1E-05)GO TO 55
    WRITE(6,94)ER(5),DS,DSTEST,B1,B2,B3,DELTAL,DELO,DELTAU
    WRITE(6,91)NIR,NIS
    GO TO 71
32  C3=DS*DDDS
    D3=DS*DRODS
    E3=DS*DXODS
    F3=DS*DFDS
    IF (NNN.EQ.0)WRITE(6,94)BLK(6),A3,B3,C3,D3,E3,F3
    RS=S+DS
    RUO=UO+A3
    IF (RUO.GT..999*AOST)GO TO 54
    RBETA=BETA+B3
    RDELTA=DELTA+C3
    RRO=R0+D3
    RXO=X0+E3
    RF=F+F3
    CALL BSR(L,LL,SI,RS)
    CALL SHOCK(RS,RUO,RBETA,RDELTA,RRO,RXO,RF)
    IF (SIN(RBETA)**2.LE..00001.OR.ABS(COS(ALAMB)).LE..00001.OR.FAC.LT.
    10.0.OR.ABS(RHOO).LE..00001.OR.ABS(RRO).LE..00001.OR.ABS(DENOM).LE.
    2.00001.OR.ABS(DENOM1).LE..00001)GO TO 71
    A4=DS*DUODS
    B4=DS*DBDS
    C4=DS*DDDS
    D4=DS*DRODS
    E4=DS*DXODS
    F4=DS*DFDS
    IF (NNN.EQ.0)WRITE(6,94)BLK(7),A4,B4,C4,D4,E4,F4
    UO=UO+1./6.*(A1+2.*A2+2.*A3+A4)
C  TEST FOR VELOCITY DECREASE
    IF (ABS(UO).LE..00001)GO TO 530
    IF (UO)530,530,51
C  TEST FOR VELOCITY BRACKET NEAR SONIC POINT
51  IF (ABS(UO-TEST).LE..00001)GO TO 53

```

APPENDIX C

```

IF(UO-TEST)52,53,53
52 IF(S.EQ.0.0)DSC=DS
S=S+DS
HUO=UO
BETA=BETA+1./6.*(B1+2.*B2+2.*B3+B4)
DELTA=DELTA+1./6.*(C1+2.*C2+2.*C3+C4)
RO=RO+1./6.*(D1+2.*D2+2.*D3+D4)
IF(RO.GT.R.AND.L.GT.1.AND.LN.EQ.1) GO TO 530
XO=XO+1./6.*(E1+2.*E2+2.*E3+E4)
F=F+1./6.*(F1+2.*F2+2.*F3+F4)
N=1
NIS=NIS+1
C INCREASE STEP SIZE IF INTEGRATION SMOOTH ENOUGH
IF(DSTEST.GT..005.OR.ABS(S-SI).LE..1E-05.OR.LLLL.GT.1)GO TO 55
DS=1.9*DS
GO TO 55
C DELO TOO LARGE - HALVING MODE IF LOWER BOUND IS KNOWN
530 DELTAU=DELO
DELO=.5*(DELTAU+DELTAL)
IF(ABS(DELO-DELTAL).LE..1E-05.AND.LLLL.EQ.1)GO TO 5300
C SET LLLL TRIGGER - UPPER AND LOWER BOUNDS FOR DELO FOUND - START HALVING MODE
LLLL=2
GO TO 2
C SEARCH AGAIN FOR LOWER BOUND FOR DELO
5300 DELO=.5*DELO
DELTAL=DELO
GO TO 2
53 IF(ABS(UO-.999*AOST).LE..00001)GO TO 60
IF(UO-.999*AOST)60,60,54
C HALVE STEP SIZE TO ACHIEVE VELOCITY BRACKET
54 DS=DS/2.
UO=HUO
LLL=2
55 IF(S.EQ.0.0)GO TO 200
RS=S
RUO=UO
RBETA=BETA
RDELTA=DELTA
RRO=RO
RXO=XO
RF=F
GO TO 30
C VELOCITY WITHIN BRACKET - - PREPARE TO EXTRAPOLATE
60 S=S+DS
BETA=BETA+1./6.*(B1+2.*B2+2.*B3+B4)

```

APPENDIX C

```

DELTA=DELTA+1./6.*(C1+2.*C2+2.*C3+C4)
RO=RO+1./6.*(D1+2.*D2+2.*D3+D4)
XO=XO+1./6.*(E1+2.*E2+2.*E3+E4)
F=F+1./6.*(F1+2.*F2+2.*F3+F4)
NIS=NIS+1
CALL BSR(L,LL,SI,S)
CALL SHOCK(S,UO,BETA,DELTA,RO,XO,F)
IF(L.GT.1.AND.PZ1PB.LT..1)GO TO 530
IF(R*DUODS.LT..1)GO TO 530
IF(LN.EQ.0)WRITE(6,99)S,RBETAD,THETAD,XO,RO,UO,PO,RHOO,TO,DELTA,X1
1,R1,V1,U1,P1,RHO1,DS,DBDS,DUODS,POBAR,SBAR
IF(SIN(RBETA)**2.LE..00001.OR.ABS(COS(ALAMB)).LE..00001.OR.FAC.LT.
10.0.OR.ABS(RHOQ).LE..00001.OR.ABS(RRO).LE..00001.OR.ABS(DENOM).LE.
2.00001.OR.ABS(DENOM1).LE..00001)GO TO 71
C  EXTRAPOLATION TO SONIC POINT
SST=S+(AOST-UO)/(2.*DUODS)
UOST=AOST
BETAST=BETA+DBDS*(SST-S)
DELST=DELTA+DDDS*(SST-S)
ROST=RO+DRODS*(SST-S)
XOST=XO+DXODS*(SST-S)
FST=F+DFDS*(SST-S)
DS=SST-S
NIS=NIS+1
CALL BSR(L,LL,SI,SST)
CALL SHOCK(SST,UOST,BETAST,DELST,ROST,XOST,FST)
IF(LN.EQ.0)WRITE(6,99)SST,RBETAD,THETAD,XOST,ROST,UOST,PO,RHOO,TO,
1DELST,X1,R1,V1,U1,P1,RHO1,DS,DBDS,DUODS,POBAR,SBAR
IF(LN.EQ.0)WRITE(6,98)
IF(LN.EQ.0)GO TO 601
IF(L.EQ.1)GO TO 600
C  TEST FOR SONIC POINT LOCATION
IF(ABS(ROST/R-1.).LE..0001)GO TO 600
IF(ROST.GT.R)GO TO 530
IF(ROST.LT.R.AND.LLLL.EQ.1)GO TO 602
IF(ROST.LT.R.AND.LLLL.EQ.2)GO TO 603
C  CORRECT DELO FOUND - - SET LENGTH SCALE AND RERUN FOR PRINTING
600 LN=0
CD=4.*FST/ROST**2
IF(L.EQ.3)GO TO 604
IF(L.EQ.1)DELO=DELO/SST
IF(L.EQ.1)DSC=DSC/SST
SMAX=SST
GO TO 2
601 WRITE(6,100)

```

APPENDIX C

```

      GO TO 71
C   DELO TOO SMALL - - SEARCH AGAIN FOR UPPER BOUND FOR DELO
602 DELTAL=DELO
      DELO=2.*DELO
      GO TO 2
C   DELO TOO SMALL - HALVING MODE
603 DELTAL=DELO
      DELO=.5*(DELTAL+DELTAU)
      GO TO 2
C   RESCALING SPHERE CONE TO A UNIT BASE RADIUS
604 L=4
      DELO=DELO/R
      DSC=DSC/R
      SI=SI/R
      SMAX=SST/R
      GO TO 2
70 WRITE(6,94)ERR(1),DUODS
71 CONTINUE
      GO TO 1
      END

```

```

FUNCTION COT(A)
COT=COS(A)/SIN(A)
RETURN
END

```

```

FUNCTION TAN(A)
TAN=SIN(A)/COS(A)
RETURN
END

```

```

SUBROUTINE BSR(L,LL,SI,S)
COMMON ER(12),BLK(12),BCK(12),ERR(12),THETA,THETAD,AK, RBETAD,ALAMB
1,CON1,CON2,CON3,CON4,CON5,CON6,CON7,C90,C91,NNN,U1,V1,P1,GAMMA,RHO
21,ST1,Z1,H1,R1,X1,CPhi,RHOO,PO,AOSQ,STO,PHI,DDDS,DBDS,DUODS,DRODS,
3DXODS,TO,AOST,BETA,FAC,DENOM,DENOM1,DFDS,CD,R,PU1PB,POBAR,SMAX,
4SBAR,LN,DELTAL,DELO,DELTAU,NIR,NIS,L,PZ1PB
GO TO(1,2,3,4,5),L
C   DISK
1 THETA=1.5707963
  AK=0.0
  GO TO 9

```

APPENDIX C

```

C CONVEX SPHERICAL CAP PORTION - - LENGTH SCALE IS SPHERE RADIUS
  2 THETA=1.5707963-S
  AK=1.0
  GO TO 9
C SPHERE-CONE CHECK FOR JUNCTION
  3 IF((SI-S).GT..00001)GO TO 2
  IF (ABS(S-SI).LE..00001.AND.LL.EQ.1)GO TO 6
C SPHERE-CONE BEYOND JUNCTION
  AK=0.0
  GO TO 9
C RESCALED SPHERE-CONE CHECK FOR JUNCTION
  4 IF((SI-S).GT..00001)GO TO 7
  IF (ABS(S-SI).LE..00001.AND.LL.EQ.1)GO TO 8
C RESCALED SPHERE-CONE BEYOND JUNCTION
  AK=0.0
  GO TO 9
C CONCAVE SPHERICAL CAP
  5 THETA=1.5707963+S
  AK=-1.0
  GO TO 9
C SPHERE-CONE JUNCTION REACHED
  6 LL=2
  GO TO 2
C RESCALED SPHERE-CONE ON SPHERICAL PORTION - LENGTH SCALE IS CONE BASE RADIUS
  7 THETA=1.5707963-R*S
  AK=R
  GO TO 9
C RESCALED SPHERE-CONE JUNCTION REACHED
  8 LL=2
  GO TO 7
  9 THETAD=THETA*57.295780
  RETURN
  END

```

```

SUBROUTINE SHOCK(RS,RUO,RBETA,RDELTA,RRO,RXO,RF)
COMMON ER(12),BLK(12),BCK(12),ERR(12),THETA,THETAD,AK,RBETAD,ALAMB
1,CON1,CON2,CON3,CON4,CON5,CON6,CON7,C90,C91,NNN,U1,V1,P1,GAMMA,RHO
21,ST1,Z1,H1,R1,X1,CPHI,RH00,PO,AOSQ,STO,PHI,DDDS,DBDS,DUODS,DRODS,
3DXODS,TO,AOST,BETA,FAC,DENOM,DENOM1,DFDS,CD,R,PU1PB,POBAR,SMAX,
4SBAR,LN,DELTA,DELO,DELTAU,NIR,NIS,L,PZ1PB
THETAD=THETA*57.295780
RBETAD=RBETA*57.295780
C90=1.+AK*RDELTA
C91=2.+AK*RDELTA

```

APPENDIX C

```

C SHOCK WAVE FUNCTIONS
  ALAMB=RBETA-THETA
  B=CON2*SIN(RBETA)**2
  A=.5*CON1*(B-1.)/CON2
  IF (NNN.EQ.0)WRITE (6,94)BLK(8),RS,RUO, RBETA, RDELTA, RRO, RXO, RBETAD, T
  ITHETA, AK, C90, C91, ALAMB, B, A
  IF (SIN(RBETA)**2.LE..00001.OR.ABS(COS(ALAMB)).LE..00001)GO TO 1
  U1=(1.-A)*COS(THETA)+A*COT(RBETA)*SIN(THETA)
  V1=-(1.-A)*SIN(THETA)+A*COT(RBETA)*COS(THETA)
  P1=(2.*GAMMA*B-CON3)/(GAMMA*CON4*CON2)
  RH01=CON4*B/(2.+CON3*B)
C ISENTROPE CONSTANT FOR NORMAL SHOCK
  IF (ABS(RS).EQ.0.0)CPHI=P1/RH01**GAMMA
  ST1=RH01*U1
  Z1=V1*ST1
  H1=RH01*V1
  R1=RRO+RDELTA*COS(THETA)
  X1=RXO-RDELTA*SIN(THETA)
  IF (NNN.EQ.0)WRITE (6,94)BLK(9),U1,V1,P1,RH01,ST1,Z1,H1,R1,X1
  FAC=(CON5*(1.-RUO**2)+CON6)/CPHI
  IF (FAC.LT.0.0)GO TO 2
C ISENTROPIC SURFACE PRESSURE AND DENSITY
  RH00=FAC**CON7
  PO=CPHI*RH00**GAMMA
  IF (RS.EQ.0.0)PMAX=PO
  POBAR=PO/PMAX
  IF (LN.EQ.1)SMAX=1.0
  SBAR=RS/SMAX
  IF (ABS(RH00).LE..00001)GO TO 3
  AOSQ=GAMMA*PO/RH00
  TO=CON2*AOSQ
  STO=RH00*RUO
C SHOCK PARTIAL DERIVS WRT BETA
  PU1PB=-CON1*COS(RBETA)*SIN(ALAMB)-A*SIN(THETA)/SIN(RBETA)**2
  PV1PB=CON1*COS(RBETA)*COS(ALAMB)-A*COS(THETA)/SIN(RBETA)**2
  PP1PB=CON1*SIN(RBETA)*COS(RBETA)
  PRO1PB=RH01**2*4.*COT(RBETA)/(CON4*B)
  PZ1PB=H1*PU1PB+ST1*PV1PB+U1*V1*PRO1PB
  IF (L.GT.1.AND.PZ1PB.LT..1)GO TO 7
  DENOM5=RH01*CPHI
  IF (ABS(RH01).LE..00001.OR.ABS(P1).LE..00001.OR.ABS(DENOM5).LE..000
101)GO TO 8
  DISC1=P1/DENOM5
  IF (DISC1.LT.0.0)GO TO 9
  TAU1=DISC1**CON7

```

APPENDIX C

```

    TAU0=RH00
    PTAUPB=TAU1/CON3*(PP1PB/P1-PRO1PB/RH01)
    PU1T1B=U1*PTAUPB+TAU1*PU1PB
    IF(RS.EQ.0.0)GO TO 7
    IF(ABS(RRO).LE.1.E-13)GO TO 4
C  DERIVATIVES WRT S
    DDDS=C90*TAN(ALAMB)
    PHI=RDELTA*SIN(THETA)/RRO
    IF(NNN.EQ.0)WRITE(6,94)BLK(10),FAC,RH00,PO,AOSQ,TO,STO,PHI
    C92=R1/RRO
    DENOM=RDELTA*C92*PZ1PB
    IF(NNN.EQ.0)WRITE(6,94)BLK(11),PU1PB,PV1PB,PP1PB,PRO1PB,PZ1PB,DDDS
1, C92,DENOM
    IF(ABS(DENOM).LE..00001)GO TO 5
    FAC1=C90*(TAN(ALAMB)-PHI)*Z1-C91*C92*V1*H1+AK*RDELTA*RUO*STO+(C90+
1C92)*(PO-P1)
    DBDS=FAC1/DENOM
    DENOM1=RDELTA*TAU0*(AOSQ-RUO**2)
    IF(NNN.EQ.0)WRITE(6,94)BLK(12),FAC1,DBDS,DENOM1,RH01,P1,RH00,DISC1
1,TAU1,TAU0,PTAUPB,PU1T1B
    DRODS=SIN(THETA)
    DXODS=COS(THETA)
    DFDS=(PO-CON5)*RRO*SIN(THETA)
    IF(ABS(DENOM1).LE..00001)GO TO 7
    FAC2=C92*(RDELTA*PU1T1B*DBDS+C91*TAU1*V1)+(RUO*TAU0-U1*TAU1)*DDDS+
1PHI*(RUO*TAU0+C90*U1*TAU1)
    DUODS=-AOSQ*FAC2/ABS(DENOM1)
    GO TO 7
1 WRITE(6,94)ER(6),RBETA,ALAMB
    GO TO 7
94 FORMAT(1X1A6/(8E16.8))
2 WRITE(6,94)ER(7),FAC
    GO TO 7
3 WRITE(6,94)ER(8),FAC,RH00,PO
    GO TO 7
4 WRITE(6,94)ER(9),FAC,RH00,PO,AOSQ,TO,STO,RRO
    GO TO 7
5 WRITE(6,94)ER(10),DENOM,PZ1PB,DELTAL,DELO,DELTAU
    WRITE(6,91)NIR,NIS
91 FORMAT(10I5)
    GO TO 7
8 WRITE(6,94)BCK(6),RH01,P1,DENOM5
    GO TO 7
9 WRITE(6,94)BCK(7),DISC1
7 IF(NNN.EQ.0)WRITE(6,94)BCK(1),FAC2,DUODS,DRODS,DXODS,DFDS,CD

```

APPENDIX C

RETURN
END

Input Cards for Sample Cases Described in Appendix B

```

-
ER1  ER2  ER3  ER4  ER5  ER6  ER7  ER8  ER9  ER10 ER11 ER12
BLK1 BLK2 BLK3 BLK4 BLK5 BLK6 BLK7 BLK8 BLK9 BLK10 BLK11 BLK12
BCK1 BCK2 BCK3 BCK4 BCK5 BCK6 BCK7 BCK8 BCK9 BCK10 BCK11 BCK12
ERR1 ERR2 ERR3 ERR4 ERR5 ERR6 ERR7 ERR8 ERR9 ERR10 ERR11 ERR12
  1
  1    1
14000000+01  46300000+01  10000000+01  10000000+01
  2    2
14000000+01  46300000+01  10000000+01  25882000+00
14000000+01  46300000+01  10000000+01  50000000+00
  3    2
14000000+01  46300000+01  60000000+02  40000000+01
14000000+01  46300000+01  60000000+02  50000000+02
  5    1
14000000+01  47600000+01  10000000+01  25882000+00

```

REFERENCES

1. Hayes, Wallace D.; and Probstein, Ronald F.: Hypersonic Flow Theory. Academic Press, Inc., 1959.
2. Van Dyke, Milton D.: The Supersonic Blunt-Body Problem – Review and Extension. *J. Aerosp. Sci.*, vol. 25, no. 8, Aug. 1958, pp. 485-496.
3. Lomax, Harvard; and Inouye, Mamoru: Numerical Analysis of Flow Properties About Blunt Bodies Moving at Supersonic Speeds in an Equilibrium Gas. NASA TR R-204, 1964.
4. Belotserkovskii, O. M.: Flow With a Detached Shock Wave About a Symmetrical Profile. *J. Appl. Math. Mech.*, vol. 22, no. 2, 1958, pp. 279-296.
5. Traugott, Stephen C.: An Approximate Solution of the Direct Supersonic Blunt-Body Problem for Arbitrary Axisymmetric Shapes. *J. Aerosp. Sci.*, vol. 27, no. 5, May 1960, pp. 361-370.
6. Gold, Ruby; and Holt, Maurice: Calculation of Supersonic Flow Past a Flat-Headed Cylinder by Belotserkovskii's Method. AFOSR TN-59-199, AD 211-525, U.S. Air Force, Mar. 1959.
7. Holt, Maurice: Direct Calculation of Pressure Distribution on Blunt Hypersonic Nose Shapes With Sharp Corners. *J. Aerosp. Sci.*, vol. 28, no. 11, Nov. 1961, pp. 872-876.
8. Xerikos, J.; and Anderson, W. A.: An Experimental Investigation of the Shock Layer Surrounding a Sphere in Supersonic Flow. *AIAA J.*, vol. 3, no. 3, Mar. 1965, pp. 451-457.
9. Xerikos, J.; and Anderson, W. A.: A Critical Study of the Direct Blunt Body Integral Method. Rep. SM-42603, Missile & Space Syst. Div., Douglas Aircraft Co., Inc., Dec. 28, 1962.
10. Belotserkovskii, O. M.; Sedova, E. S.; and Shugaev, F. V. (John W. Brook, transl.): Supersonic Flow About Blunt Bodies of Revolution With a Corner. Grumman Res. Dep. Transl. TR-42, Grumman Aircraft Eng. Corp., Mar. 1967.
11. Vaglio-Laurin, Roberto: Transonic Rotational Flow Over a Convex Corner. *J. Fluid Mech.*, vol. 9, pt. 1, Sept. 1960, pp. 81-103.
12. Stallings, Robert L., Jr.: Experimentally Determined Local Flow Properties and Drag Coefficients for a Family of Blunt Bodies at Mach Numbers From 2.49 to 4.63. NASA TR R-274, 1967.

13. Boison, J. Christopher; and Curtiss, Howard A.: An Experimental Investigation of Blunt Body Stagnation Point Velocity Gradient. ARS J., vol. 29, no. 2, Feb. 1959, pp. 130-135.
14. Busemann, Adolph: A Review of Analytical Methods for the Treatment of Flows With Detached Shocks. NACA TN 1858, 1949.
15. Guderley, K. Gottfried: Considerations of the Structure of Mixed Subsonic-Supersonic Flow Patterns. Tech. Rep. No. F-TR-2168-ND, Air Mater. Command, U.S. Air Force, Oct. 1947.
16. Johnston, G. W.: An Investigation of the Flow About Cones and Wedges at and Beyond the Critical Angle. Rep. No. 24, Inst. Aerophys., Univ. of Toronto, Dec. 1952.
17. South, Jerry C., Jr.: Application of Dorodnitsyn's Integral Method to Nonequilibrium Flows Over Pointed Bodies. NASA TN D-1942, 1963.
18. Kuby, W. C.: Use of the Method of Integral Relations for the Determination of the Convective Heat Flux to a Re-Entry Body. AIAA J. (Tech. Notes), vol. 4, no. 5, May 1966, pp. 947-949.
19. Traugott, Stephen C.: Some Features of Supersonic and Hypersonic Flow About Blunted Cones. J. Aerosp. Sci., vol. 29, no. 4, Apr. 1962, pp. 389-399.
20. Kaattari, George E.: Pressure Distribution on Forward Face of Blunt Bodies at Angle of Attack. J. Spacecraft Rockets (Eng. Notes), vol. 4, no. 8, Aug. 1967, pp. 1110-1112.
21. Serbin, Hyman: The High Speed Flow of Gas Around Blunt Bodies. Aeronaut. Quart., vol. IX, pt. 4, Nov. 1958, pp. 313-330.

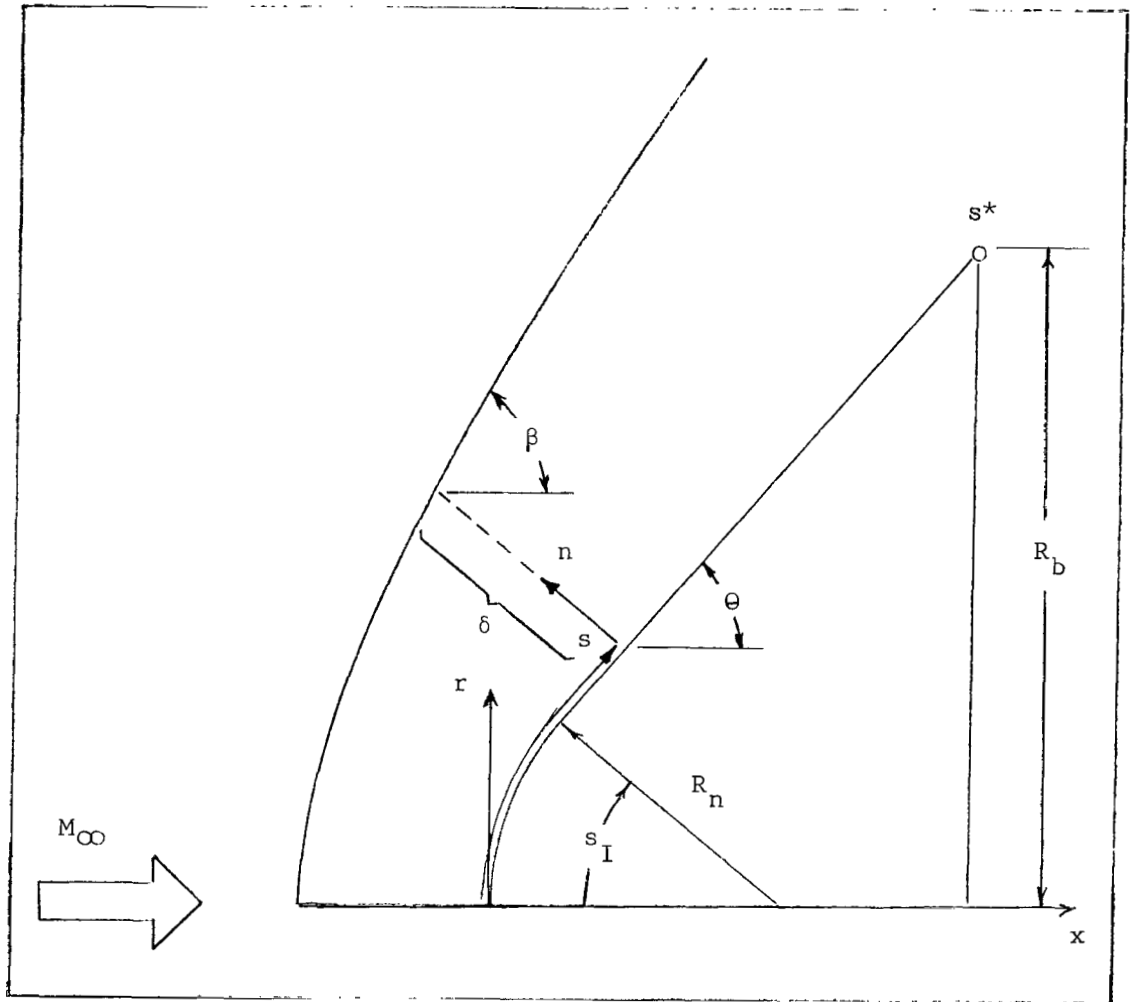


Figure 1.- Schematic of geometry and coordinates.

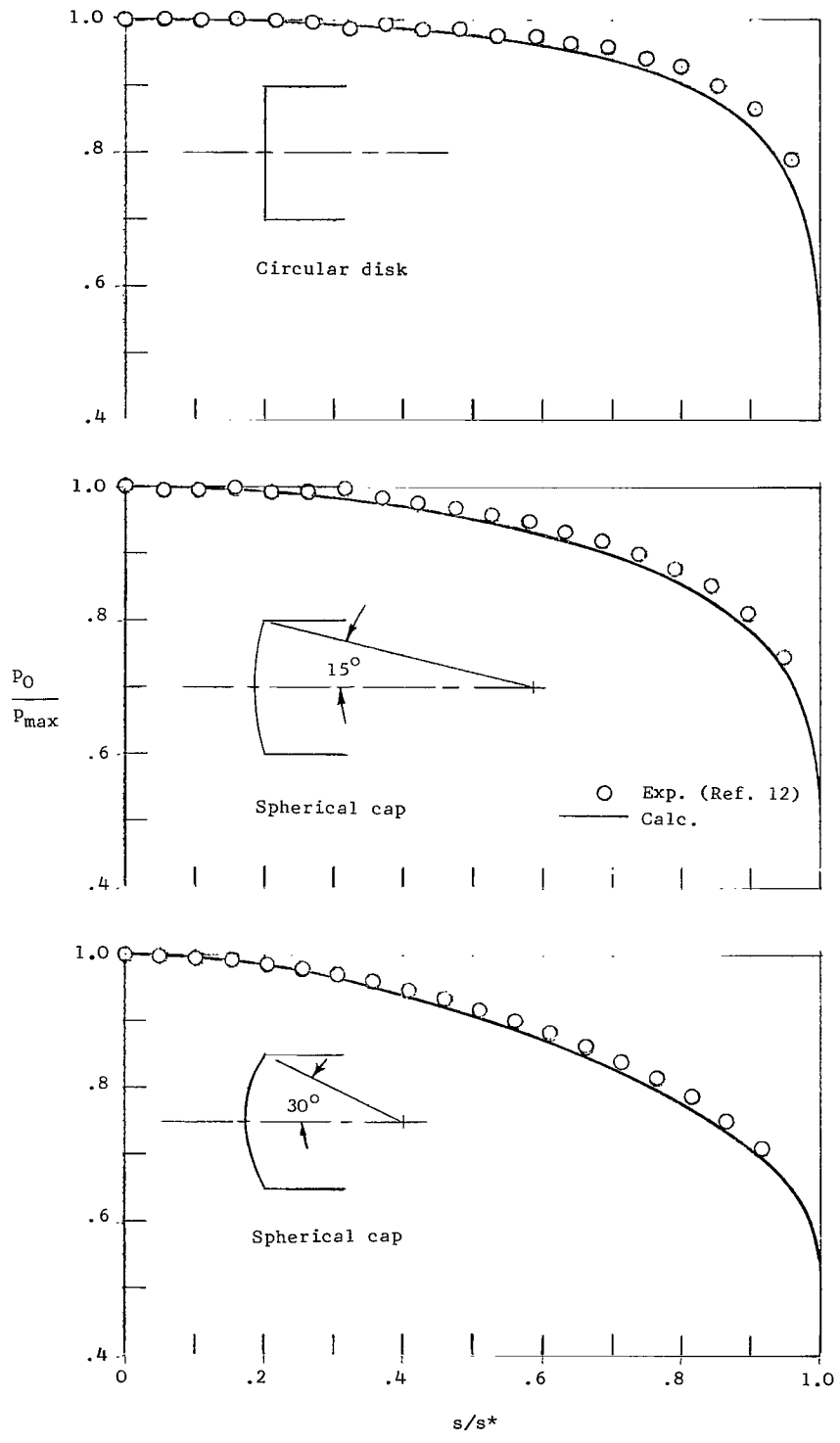


Figure 2.- Pressure distributions for a disk and two spherical caps. $\gamma = 1.4$; $M_\infty = 4.63$.

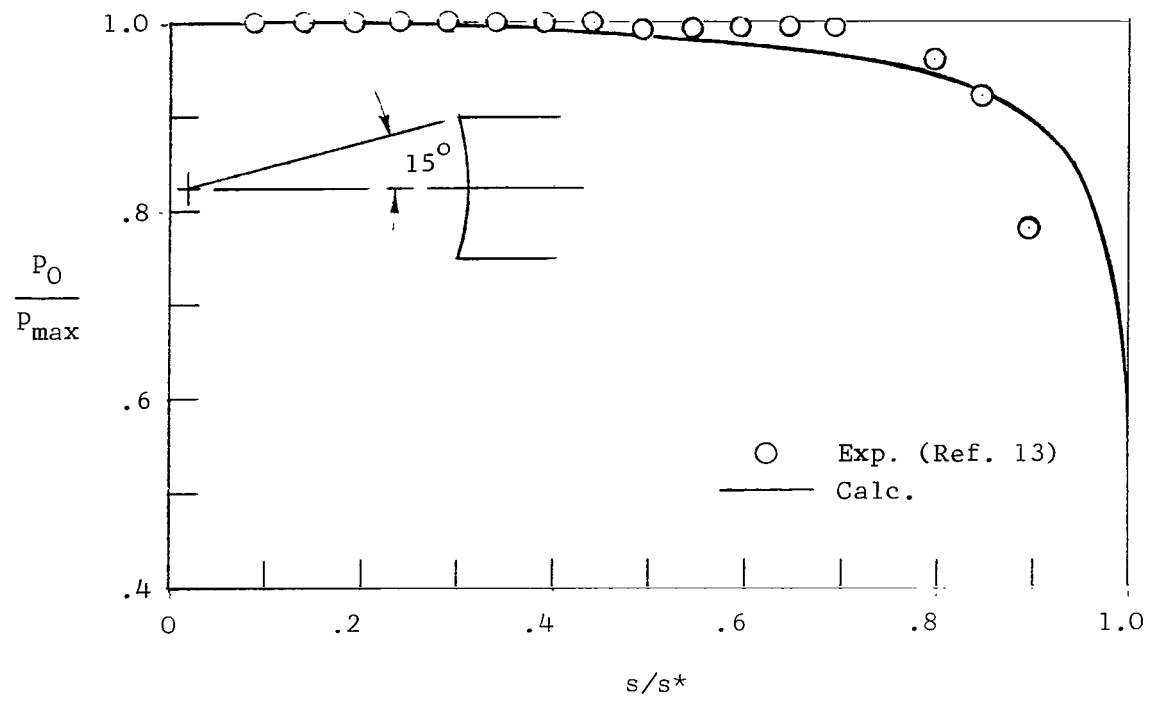
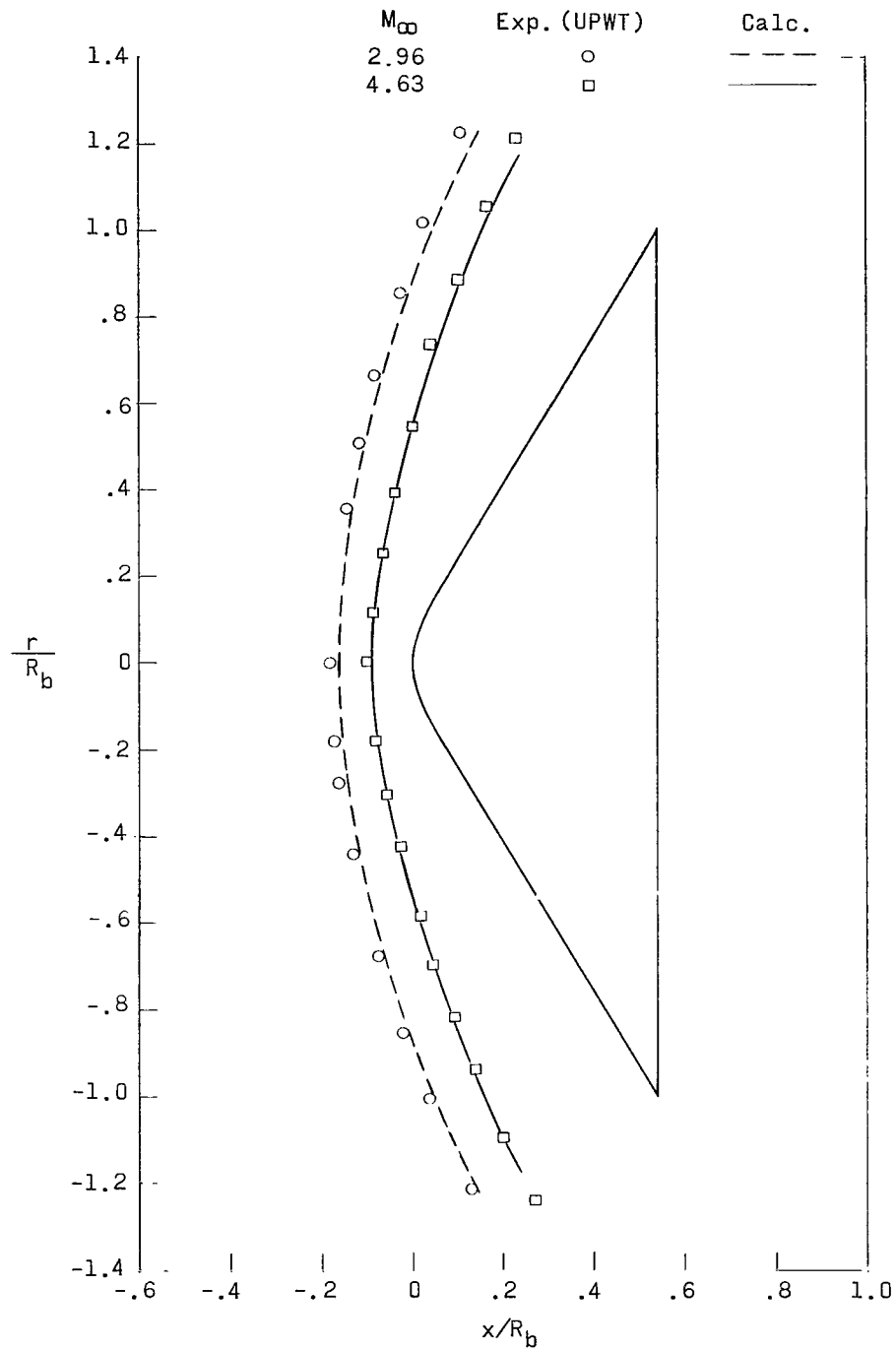
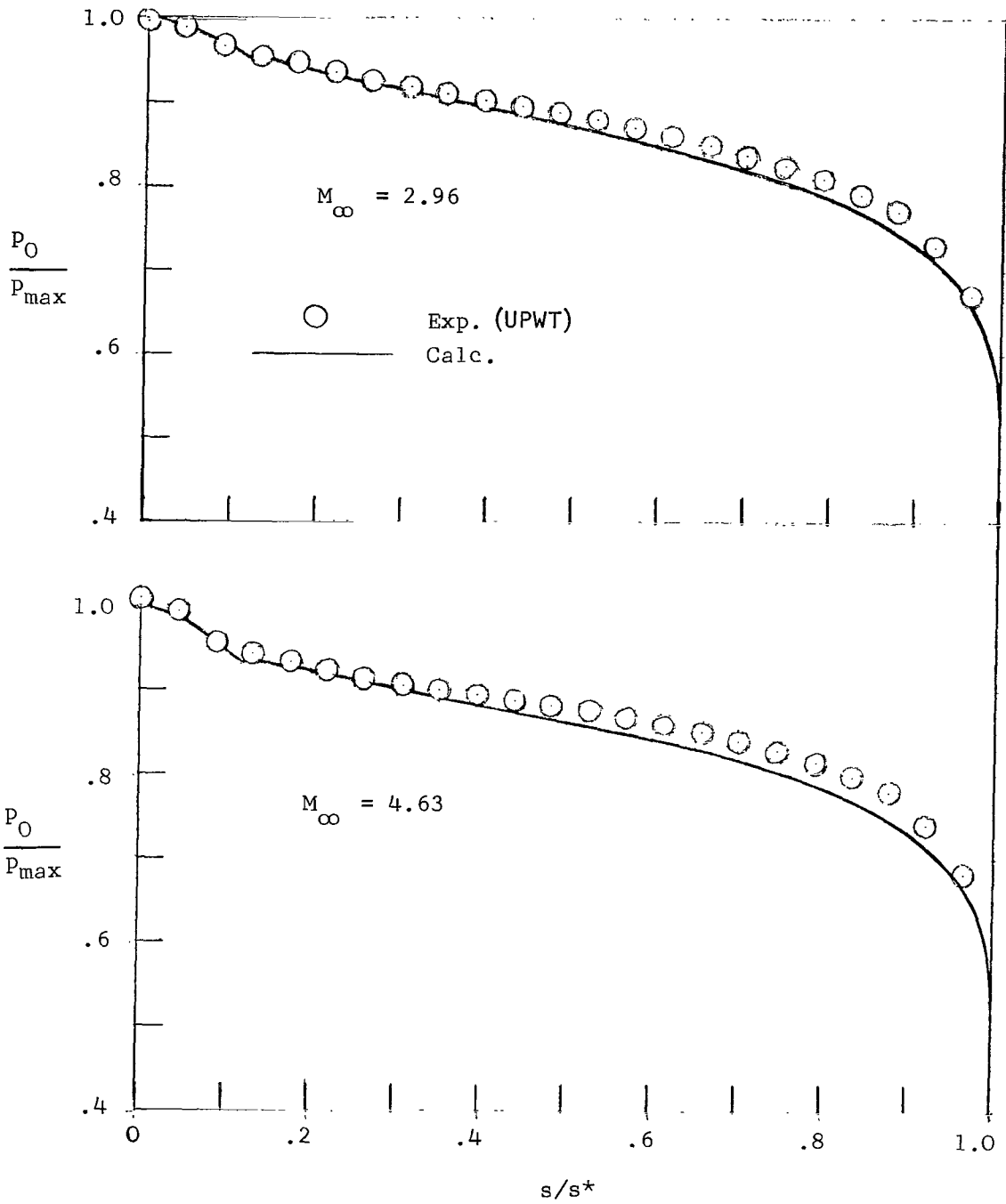


Figure 3.- Pressure distribution for a spherical cap concave to the stream. $\gamma = 1.4$; $M_\infty = 4.76$.



(a) Shock-wave shape.

Figure 4.- 60° sphere-cone. $\gamma = 1.4$; $R_n/R_b = 0.25$.



(b) Pressure distribution.

Figure 4.- Concluded.

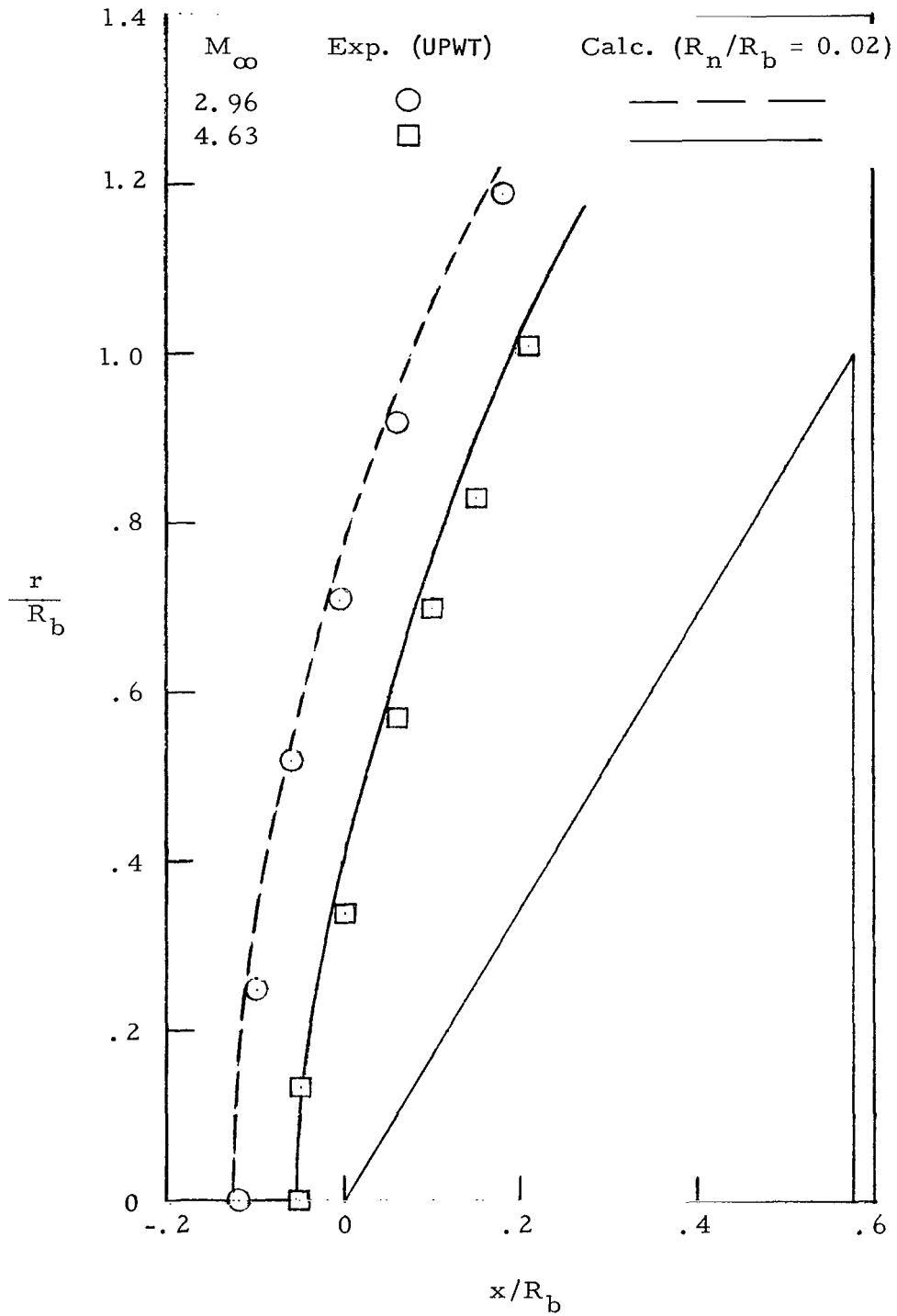


Figure 5.- Shock-wave shape for a 60° pointed cone. $\gamma = 1.4$; $R_n/R_b = 0.02$.

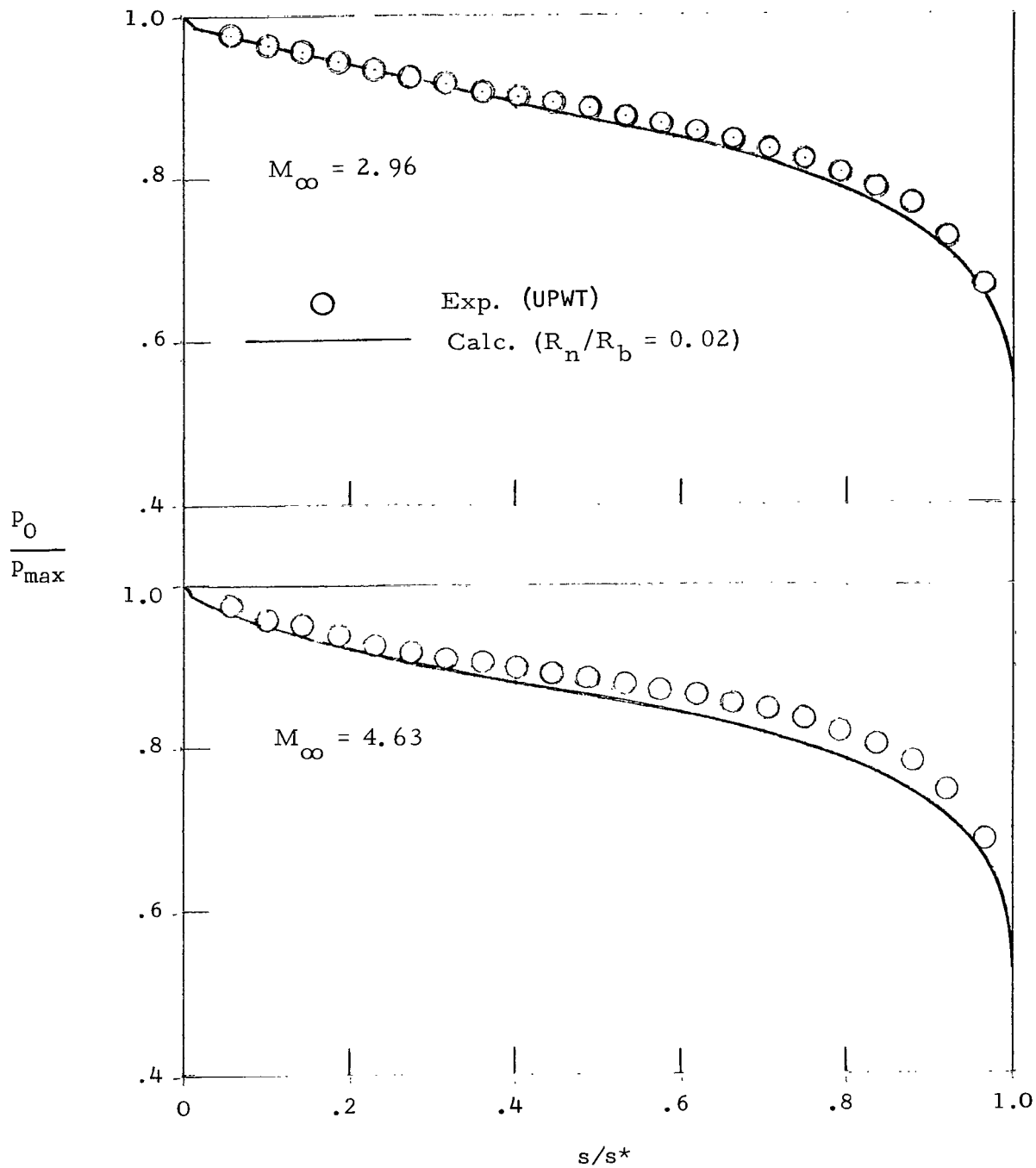
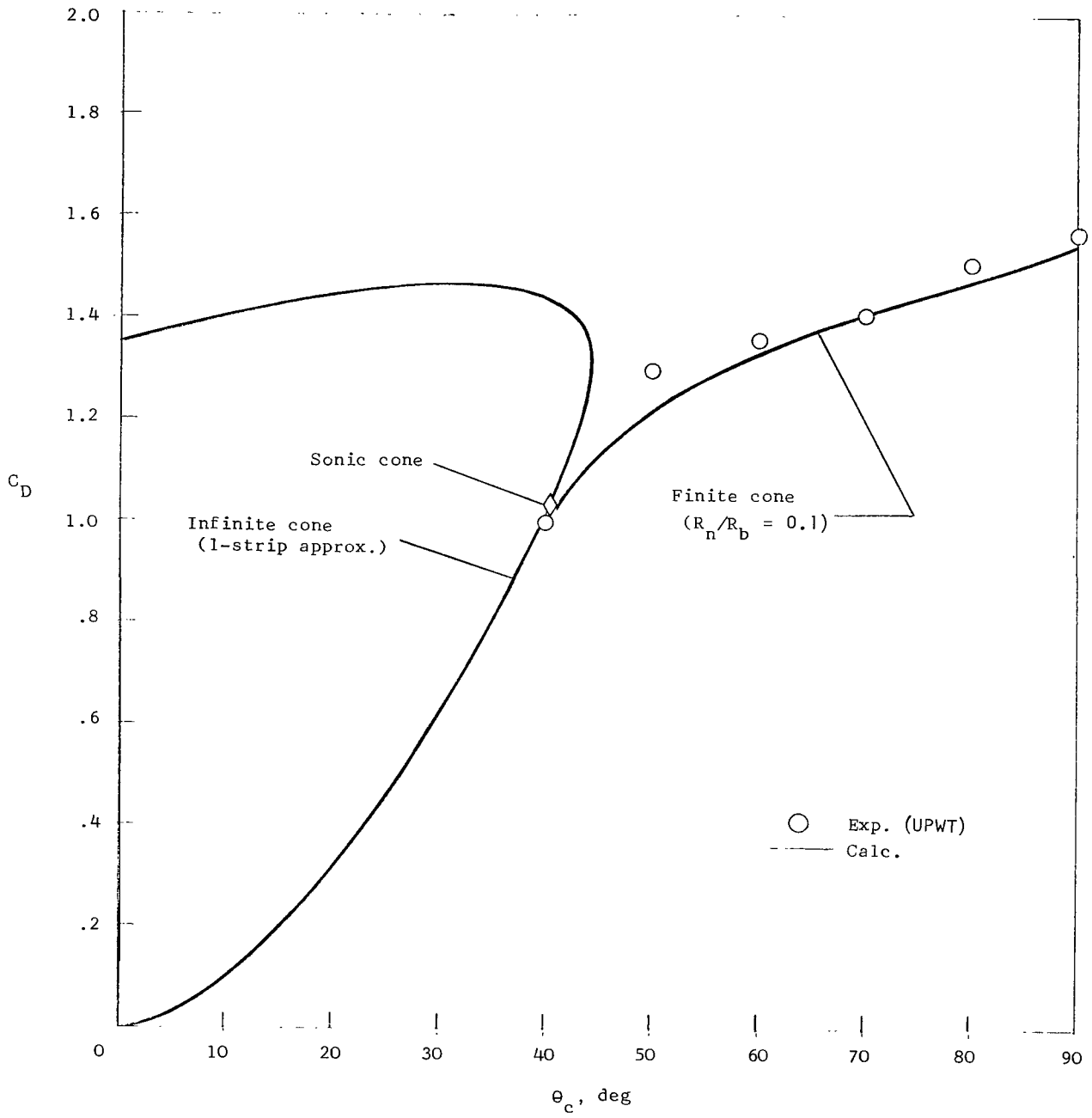
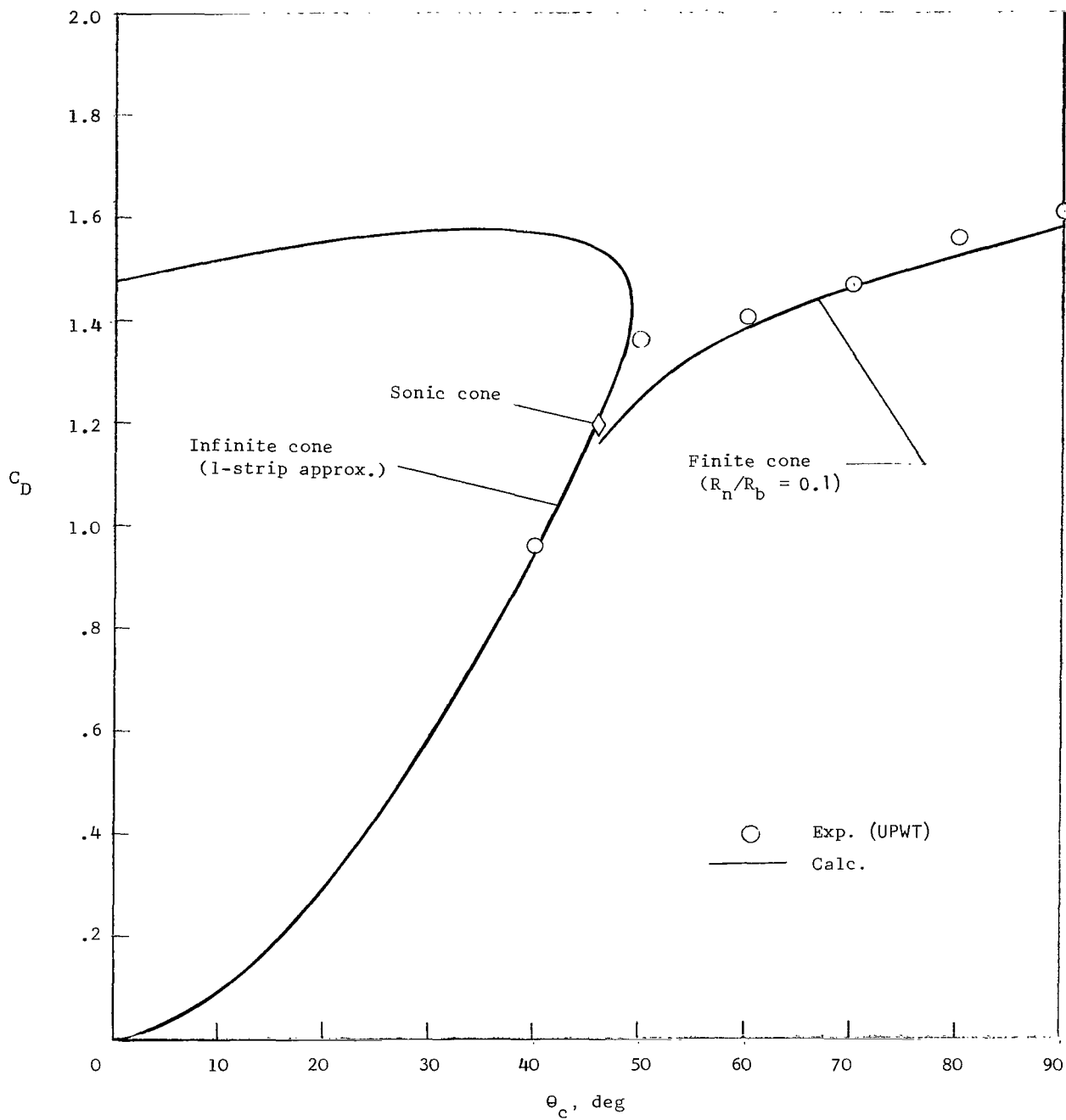


Figure 6.- Pressure distribution for a 60° pointed cone. $\gamma = 1.4$; $R_n/R_b = 0.02$.



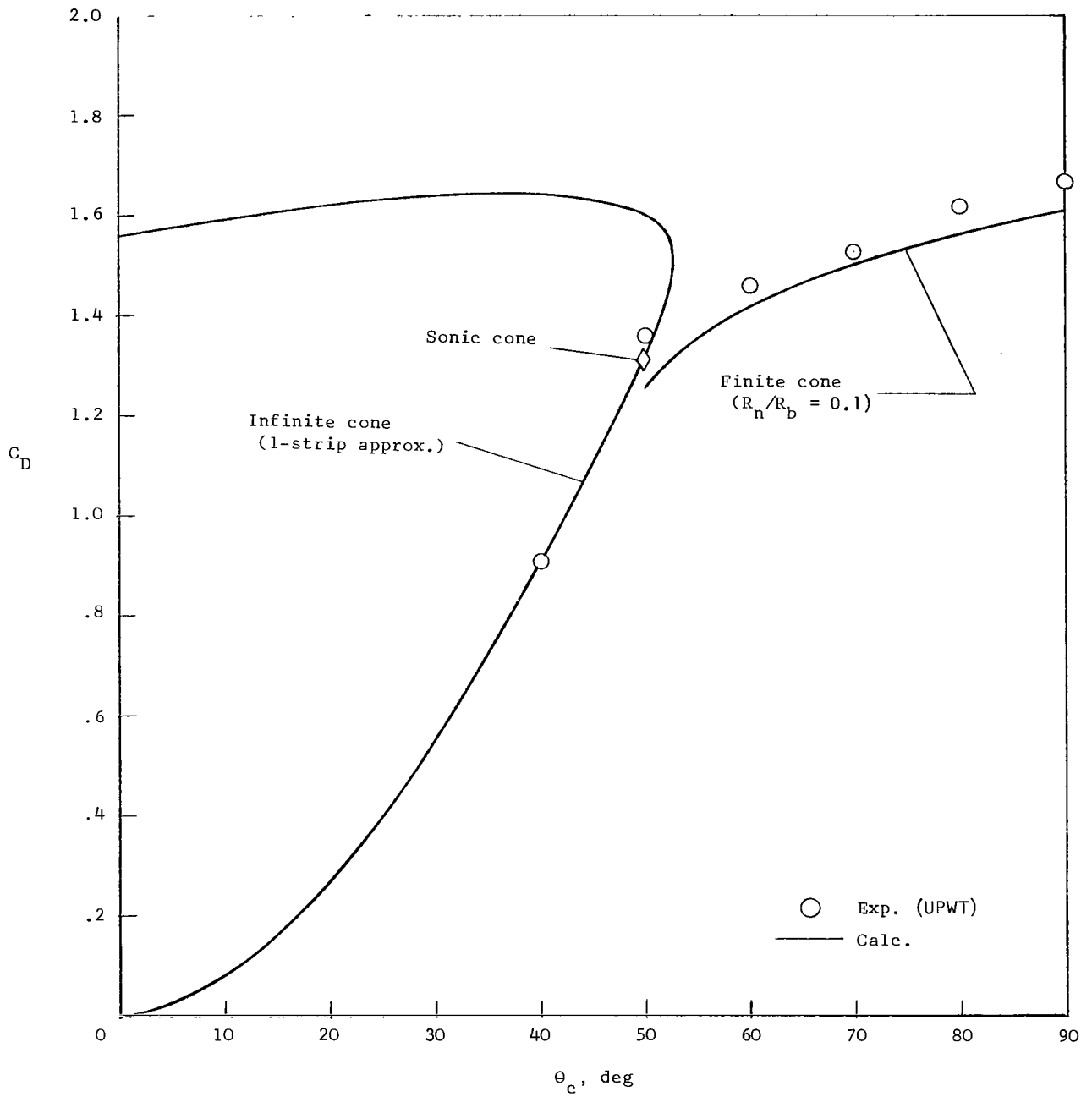
(a) $M_\infty = 2.3$.

Figure 7.- Forebody pressure drag coefficient dependence on cone angle for a pointed cone. $\gamma = 1.4$.



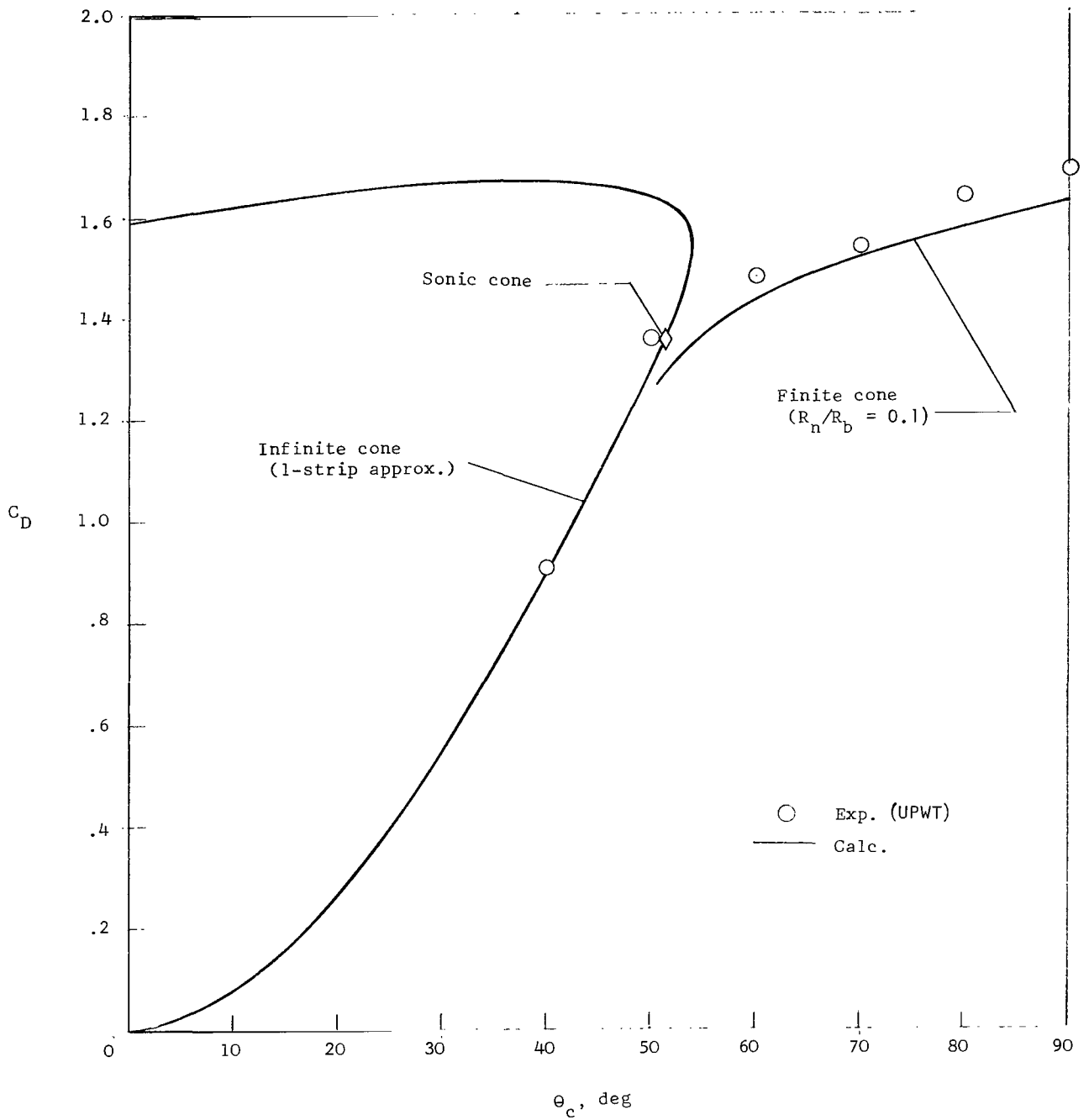
(b) $M_\infty = 2.96$.

Figure 7.- Continued.



(c) $M_\infty = 3.95$.

Figure 7.- Continued.



(d) $M_\infty = 4.63$.

Figure 7.- Concluded.

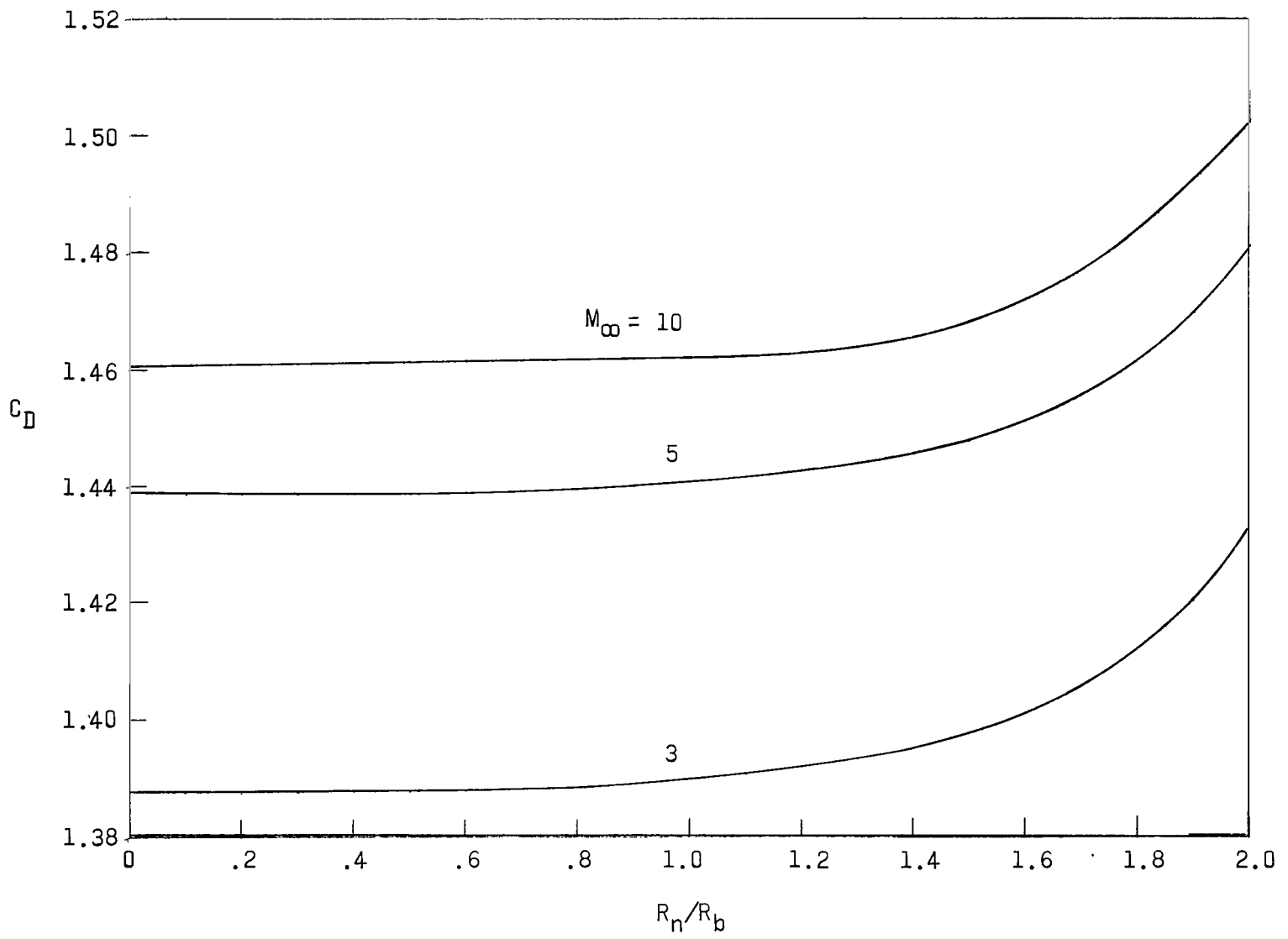


Figure 8.- Drag coefficient dependence on bluntness ratio for a 60° sphere-cone. $\gamma = 1.4$.

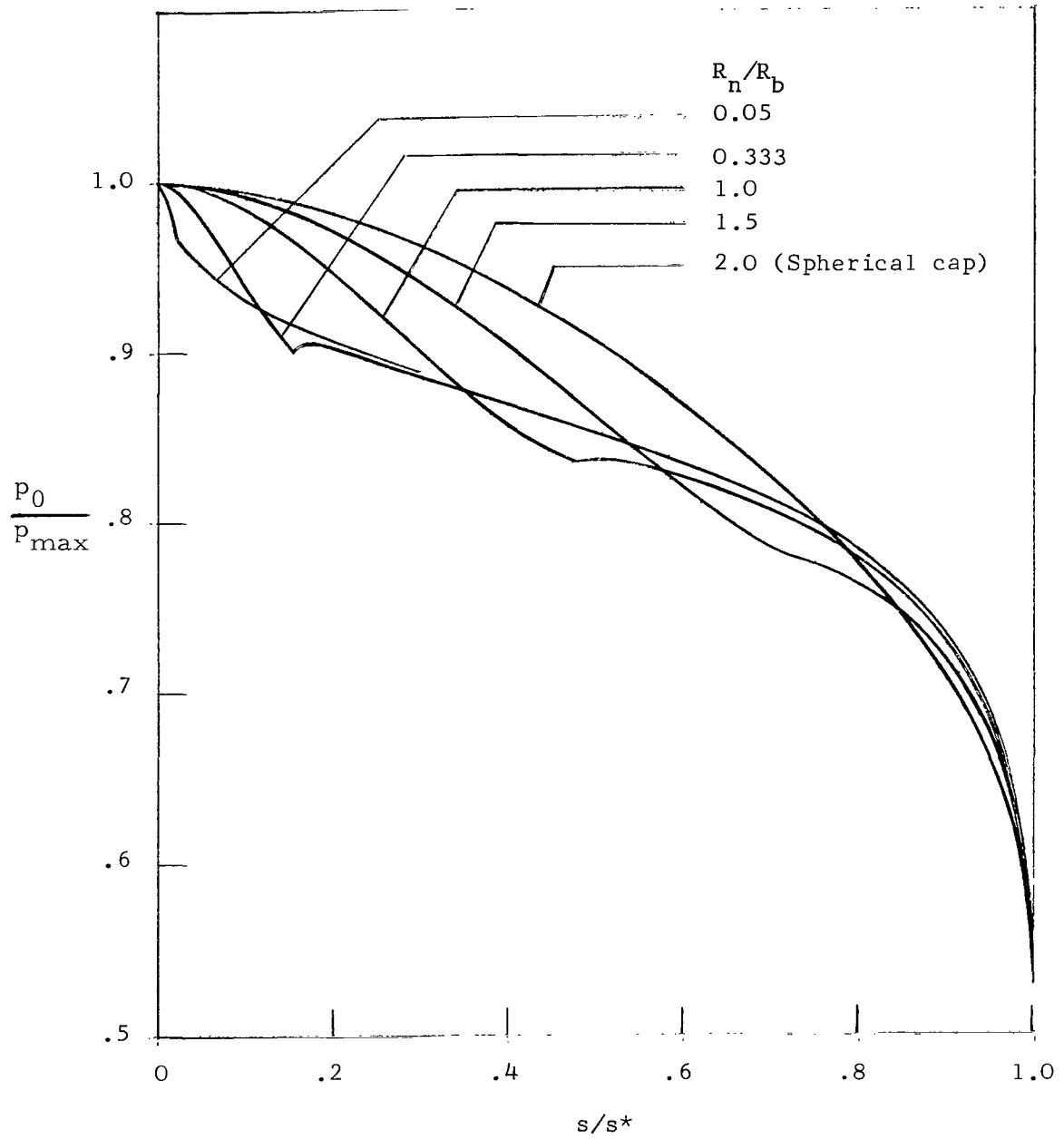


Figure 9.- Bluntness ratio effect on pressure distribution for a sphere-cone. $\gamma = 1.4$; $M_\infty = 10$; $\theta_c = 60^\circ$.

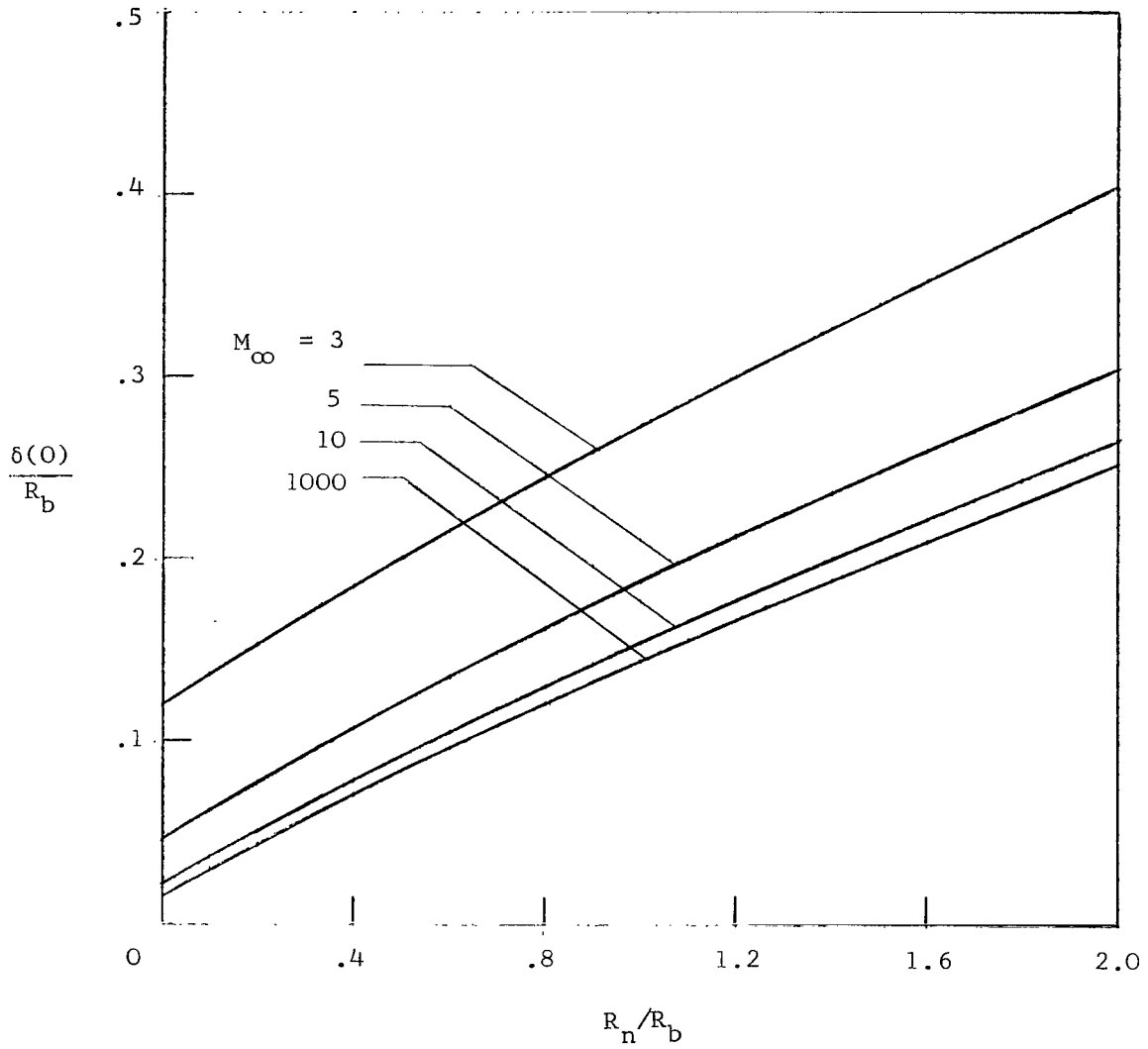


Figure 10.- Bluntness ratio effect on shock-wave standoff distance. $\gamma = 1.4$; $\theta_c = 60^\circ$.

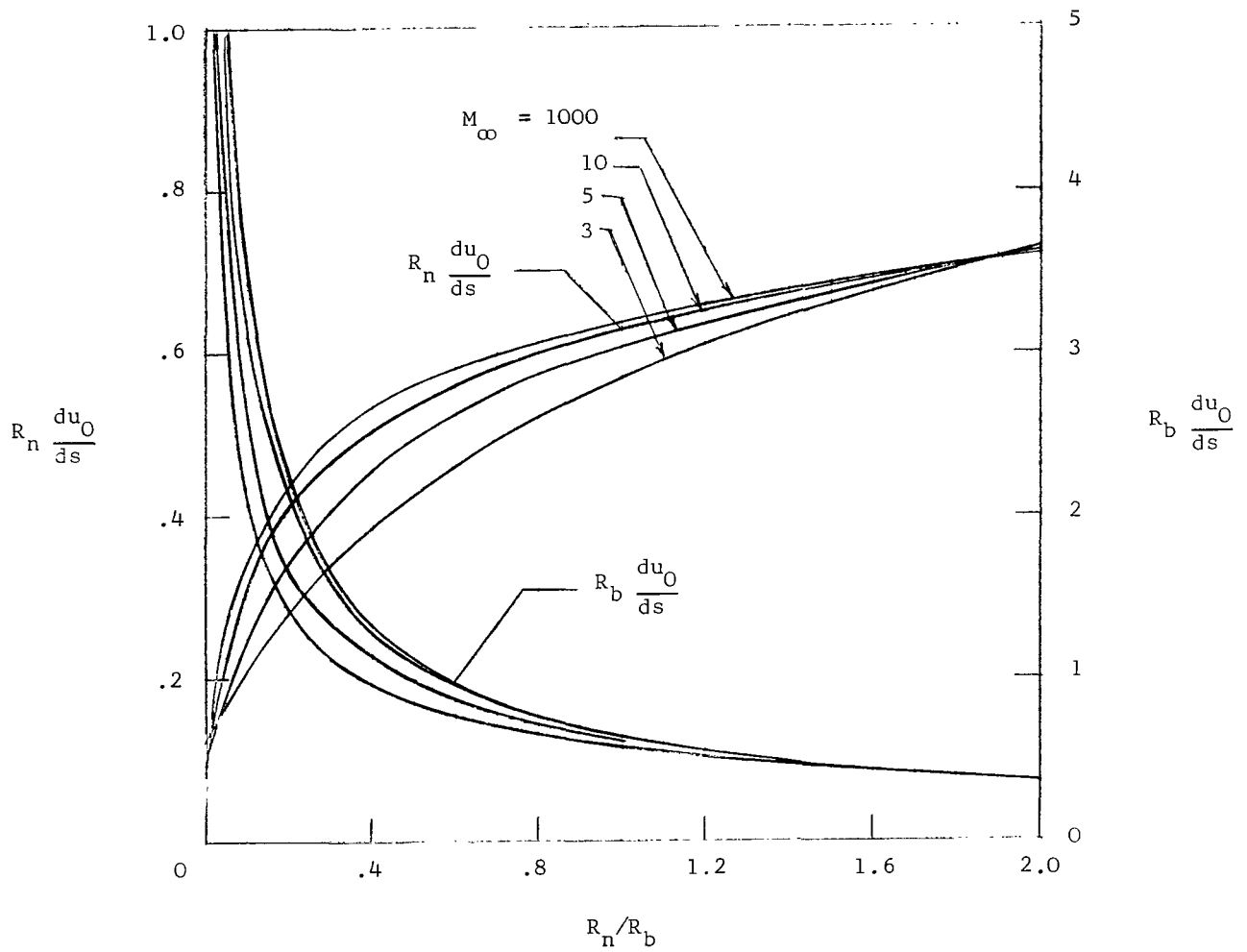


Figure 11.- Bluntness ratio effect on stagnation-point velocity gradient for a sphere-cone. $\gamma = 1.4$; $\theta_c = 60^\circ$.

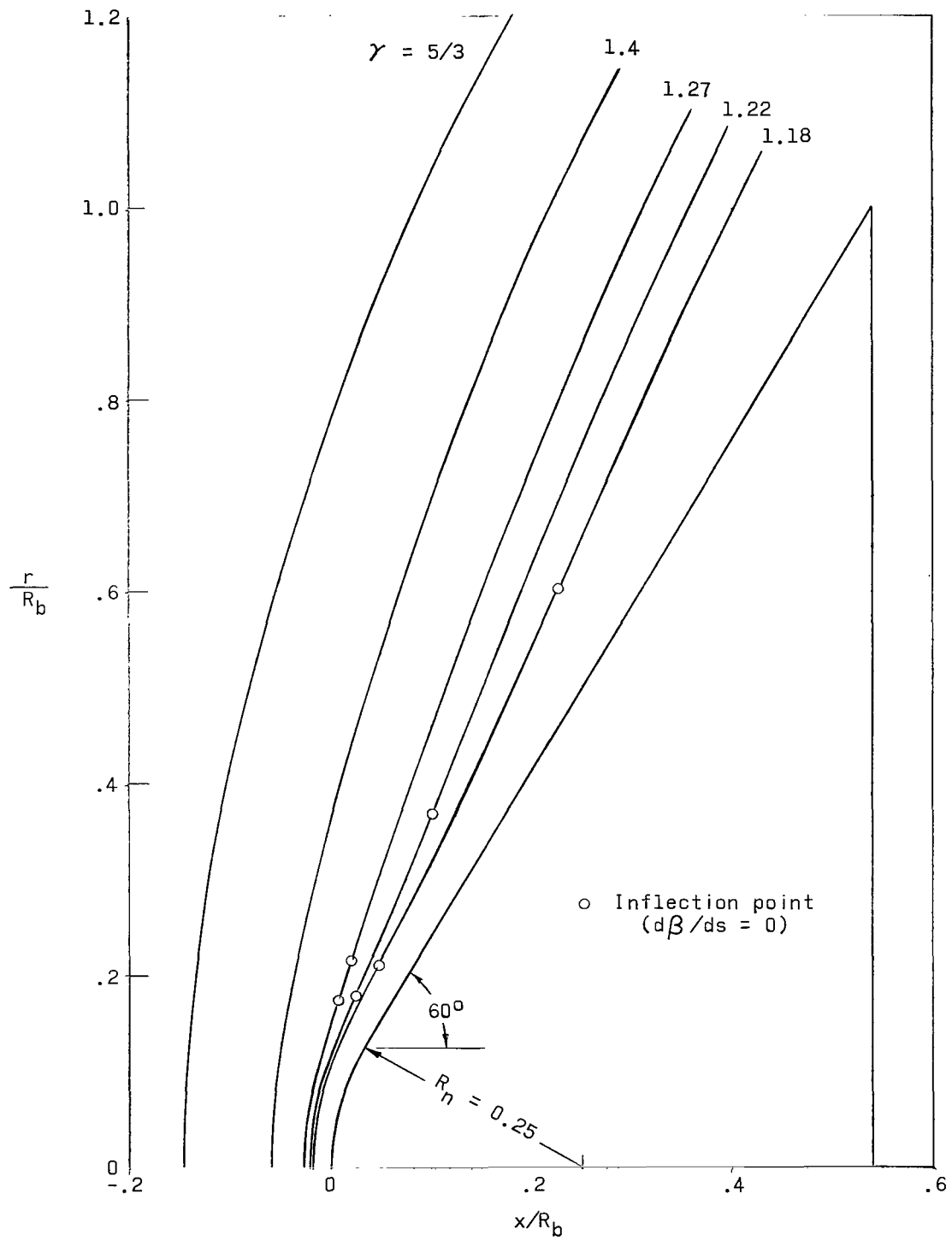


Figure 12.- Effect of γ on shock-wave shape for a sphere-cone. $M_\infty = 10$; $\theta_c = 60^\circ$; $R_n/R_b = 0.25$.

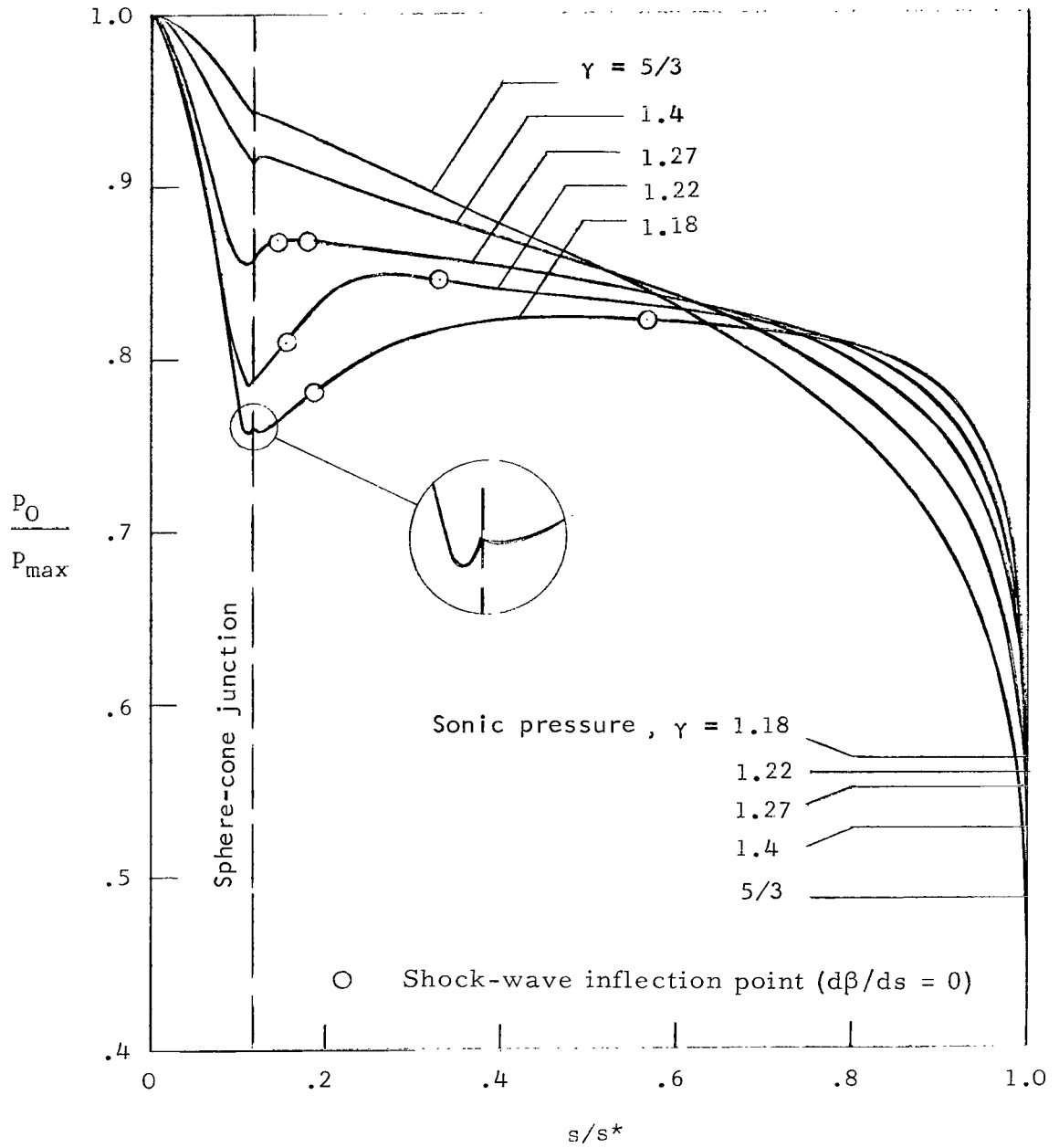


Figure 13.- Effect of γ on pressure distribution for a sphere-cone. $M_\infty = 10$; $\theta_c = 60^\circ$; $R_n/R_b = 0.25$.

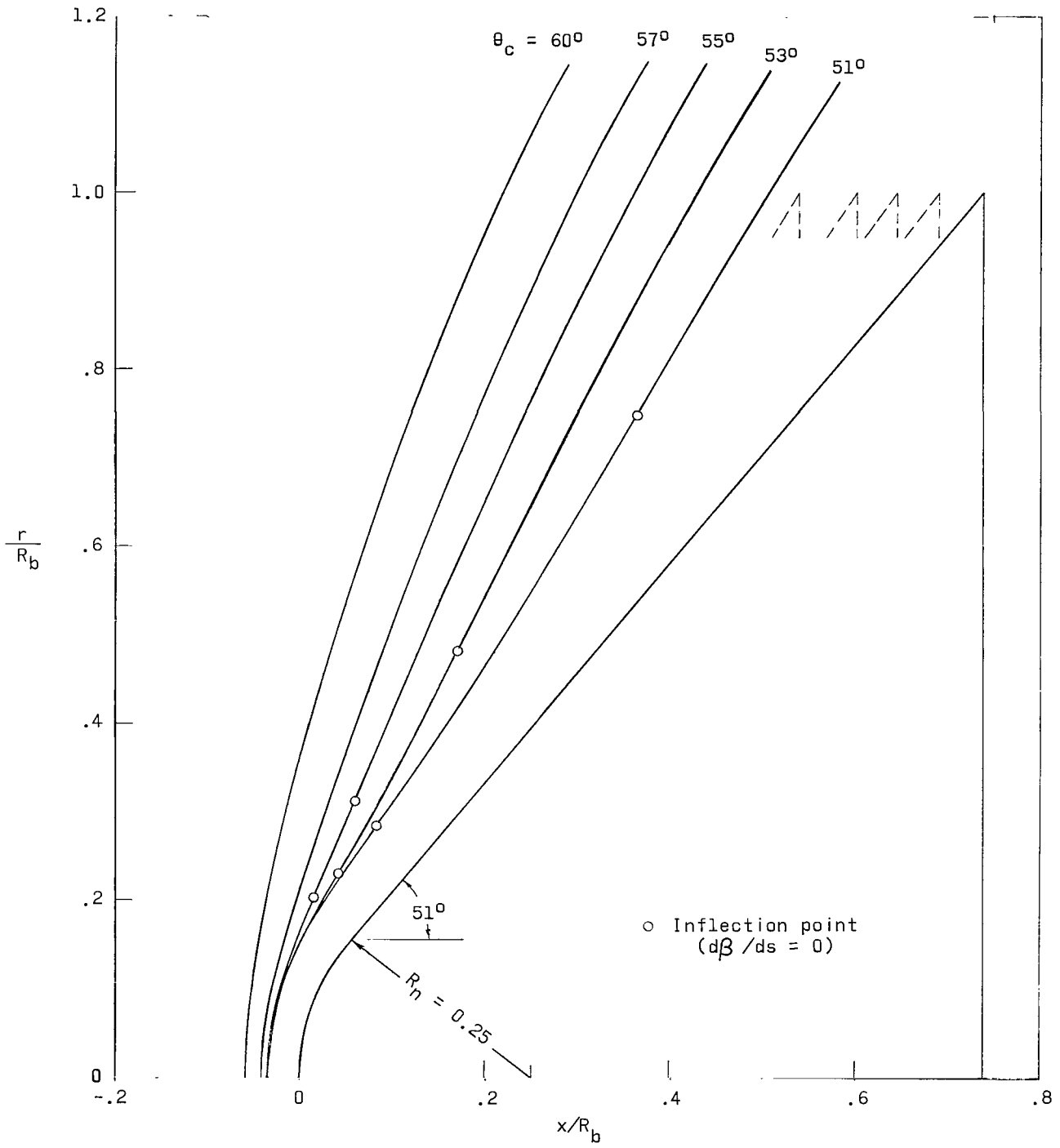


Figure 14.- Effect of θ_c on shock-wave shape for a sphere-cone. $\gamma = 1.4$; $M_\infty = 10$; $R_n/R_b = 0.25$.

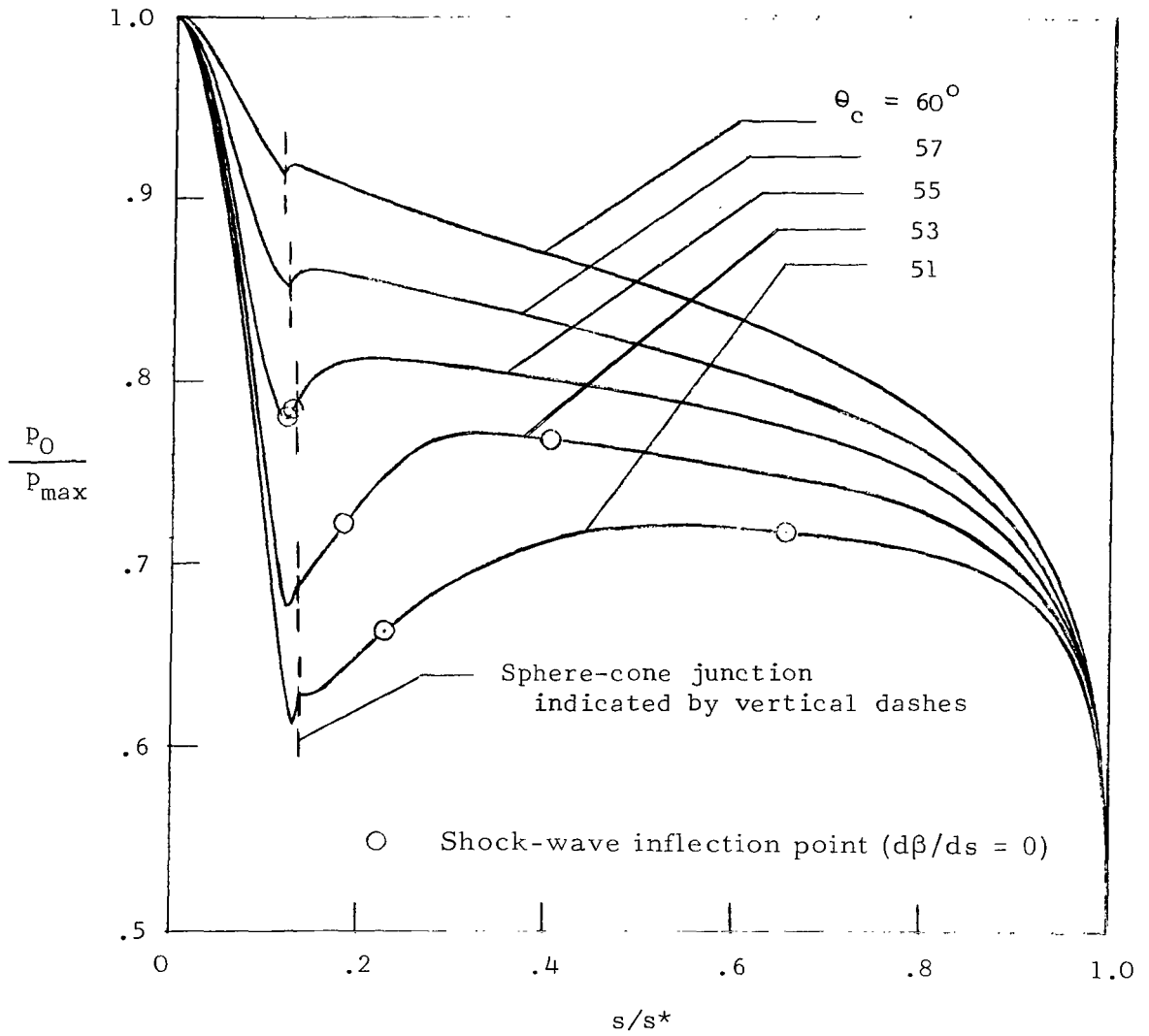


Figure 15.- Effect of θ_c on pressure distribution for a sphere-cone. $\gamma = 1.4$; $M_\infty = 10$; $R_n/R_b = 0.25$.

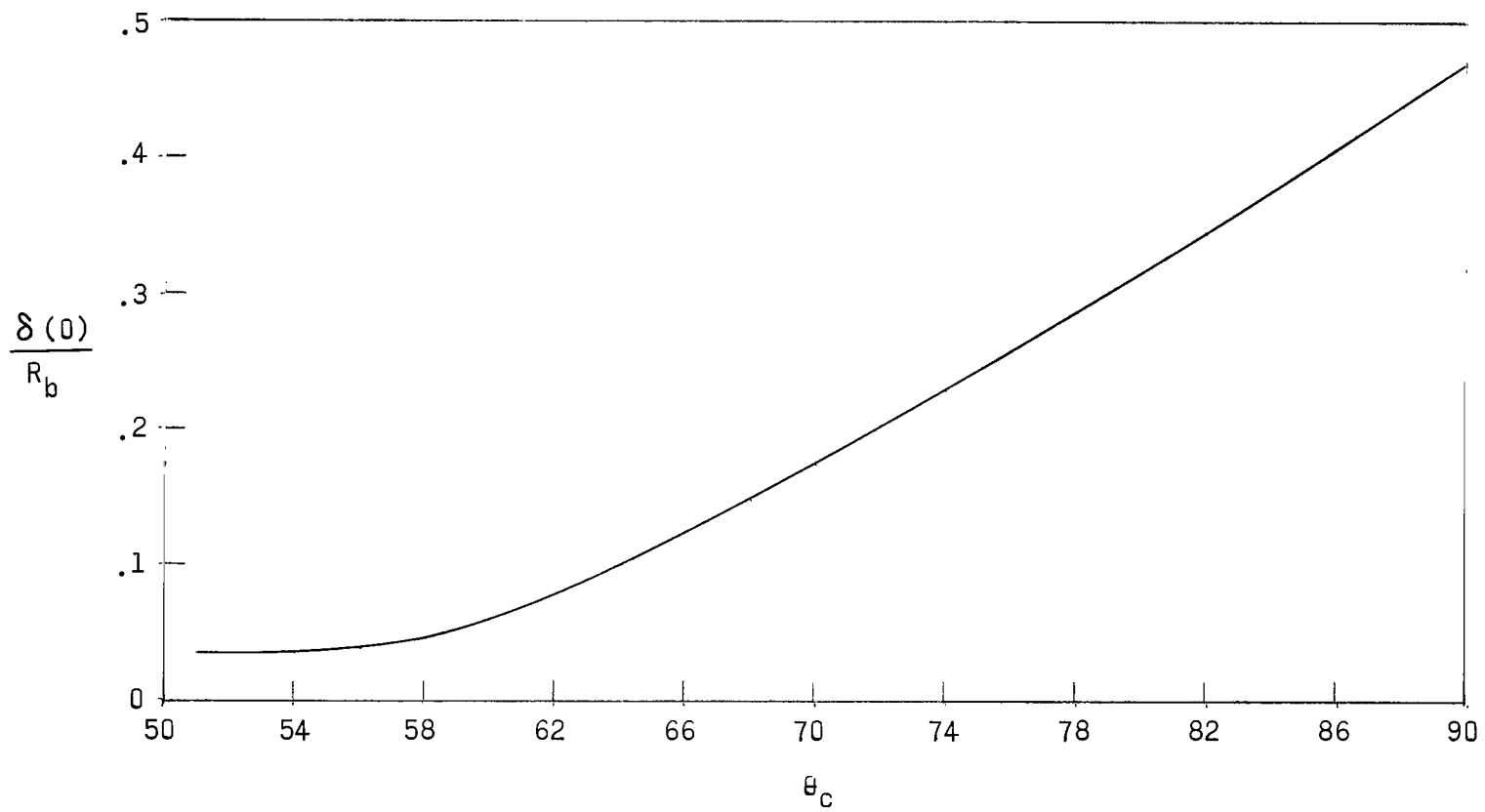


Figure 16.- Effect of θ_c on shock-wave standoff distance for a sphere-cone. $\gamma = 1.4$; $M_\infty = 10$; $R_n/R_b = 0.25$.

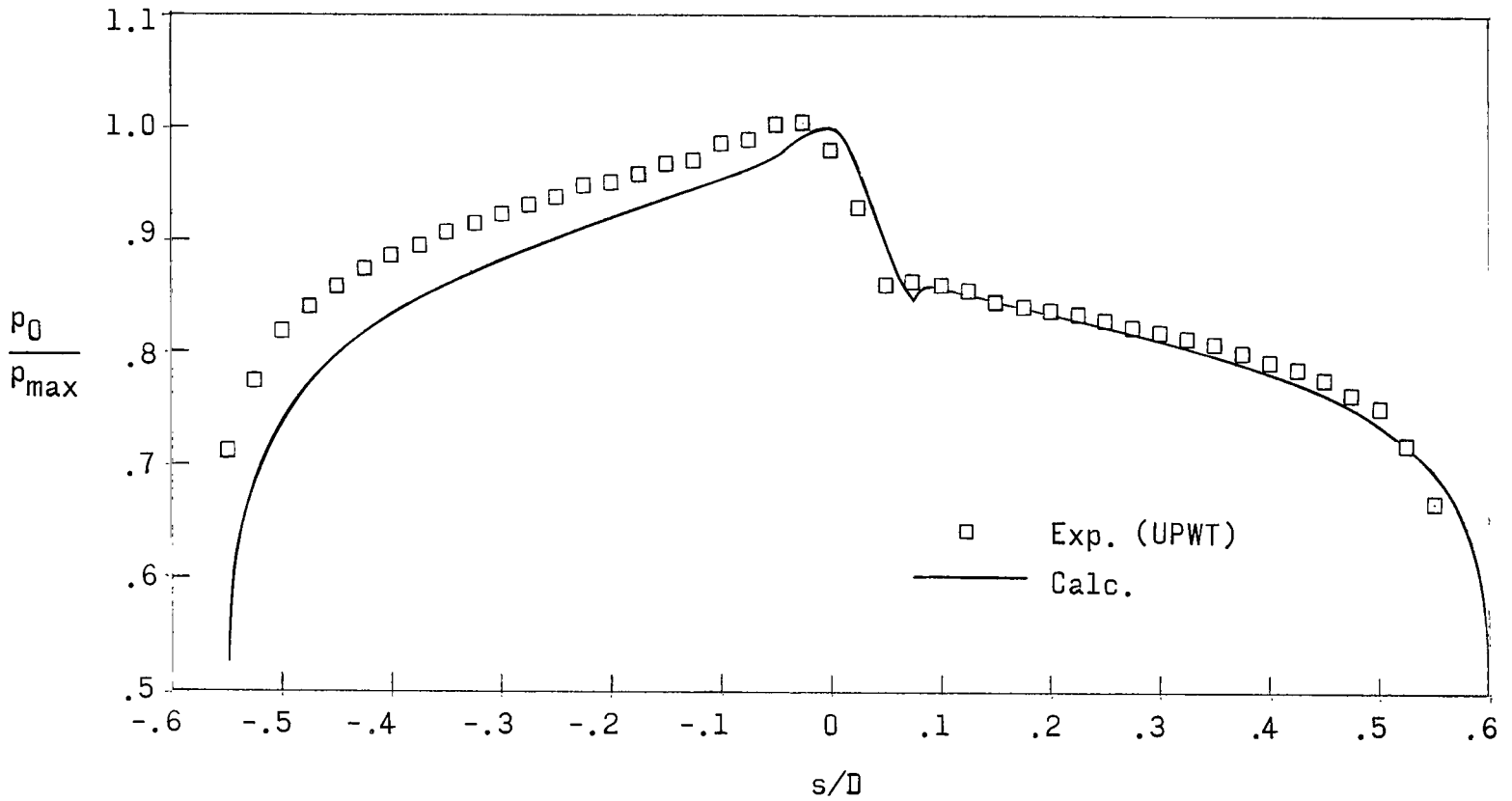


Figure 17.- Simulated pressure distributions in plane of symmetry for 60° sphere-cone at 5° angle of attack. Uncorrected s-coordinates; $\gamma = 1.4$; $M_\infty = 4.63$.

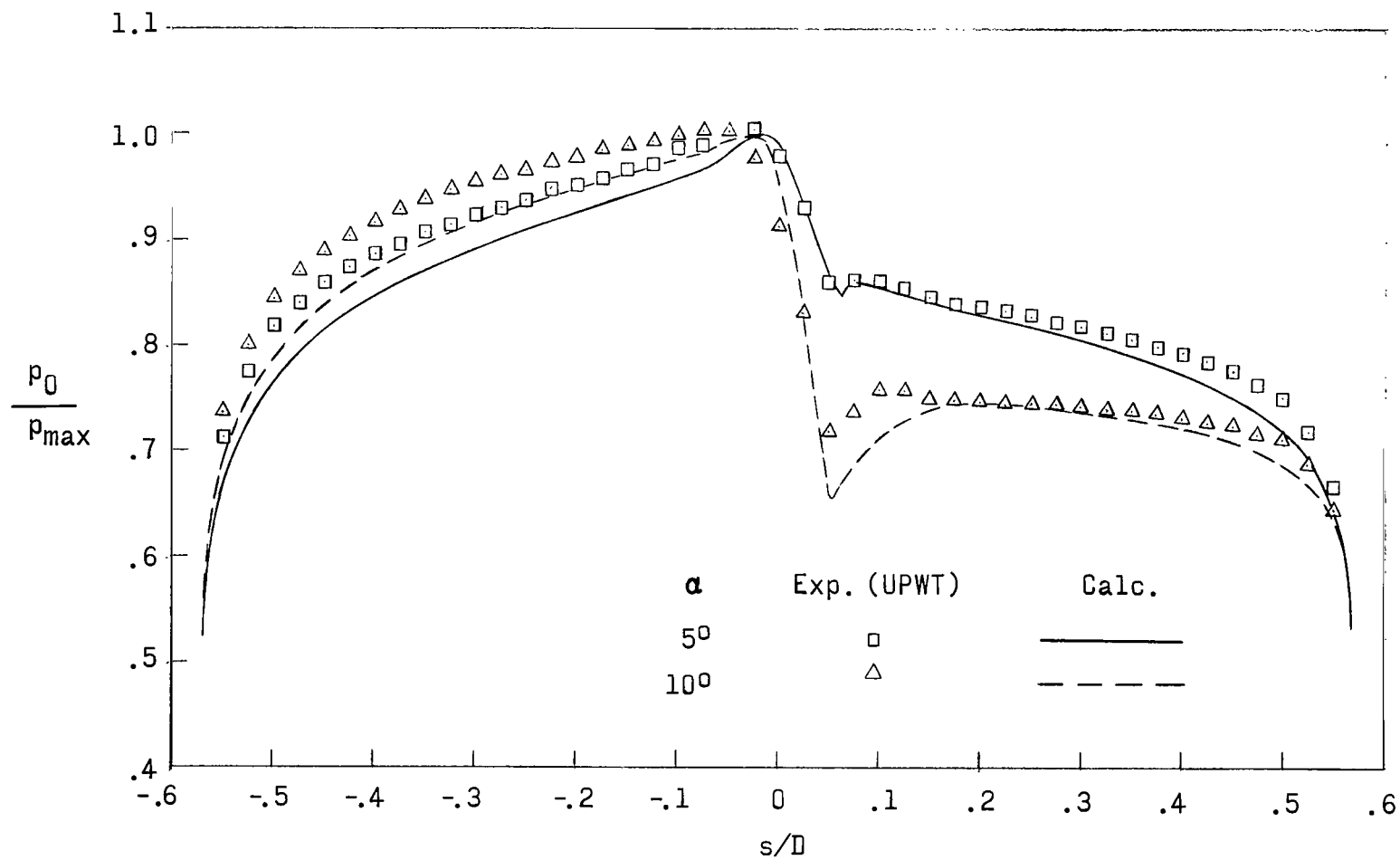


Figure 18.- Simulated pressure distribution in plane of symmetry for 60° sphere-cone at 50° and 100° angle of attack. $\gamma = 1.4$; $M_\infty = 4.63$; $R_n/R_b = 0.25$. Calculated results obtained for windward and leeward sides by respectively adding or subtracting angle of attack from nominal (60°). Then s -coordinates are shifted and stretched to correct the locations of stagnation and sonic points (see text).

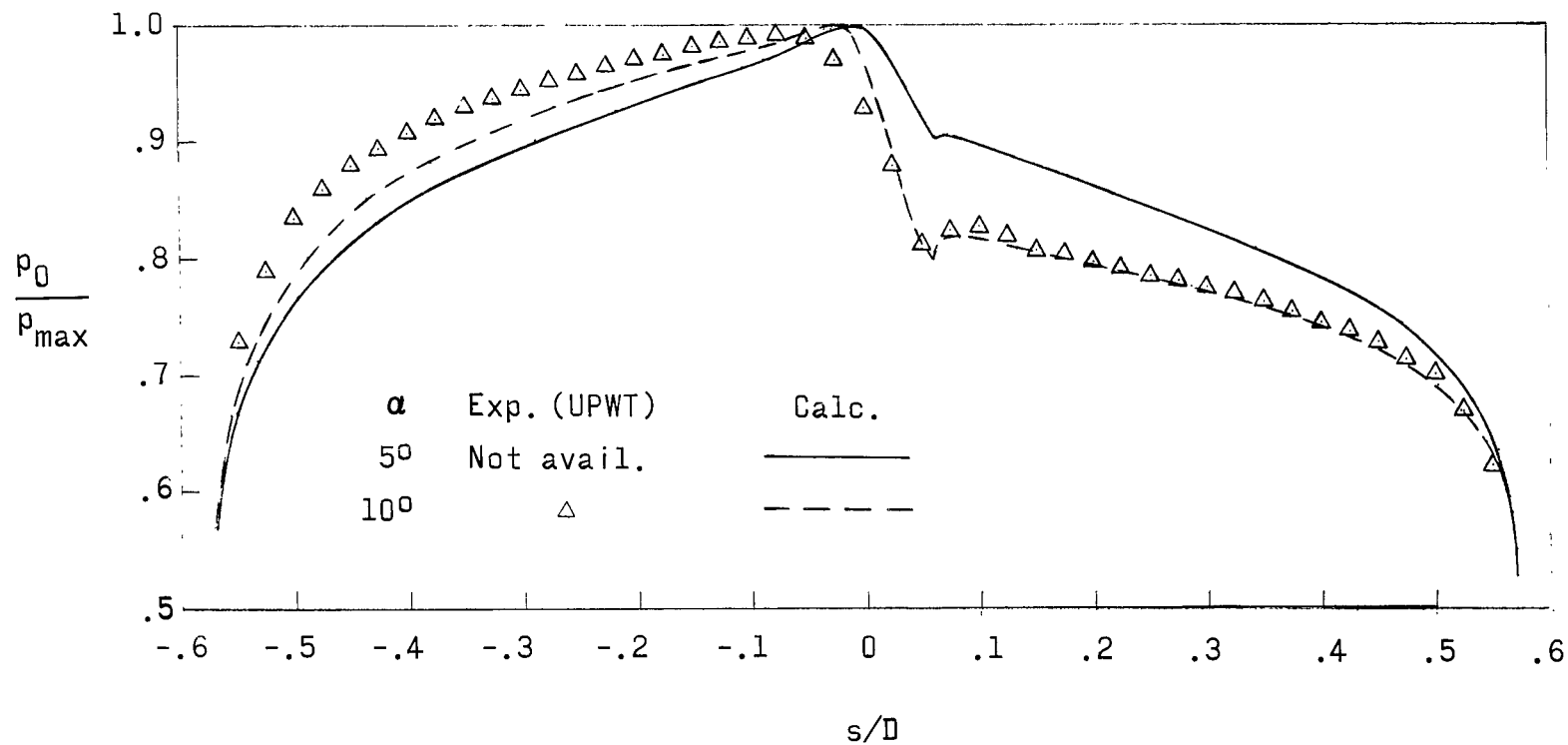


Figure 19.- Simulated pressure distribution in plane of symmetry for 60° sphere-cone at 5° and 10° angle of attack. $\gamma = 1.4$; $M_\infty = 2.96$; $R_n/R_b = 0.25$. Calculated results obtained for windward and leeward sides by respectively adding or subtracting angle of attack from nominal (60°). Then s -coordinates are shifted and stretched to correct the locations of stagnation and sonic points (see text).

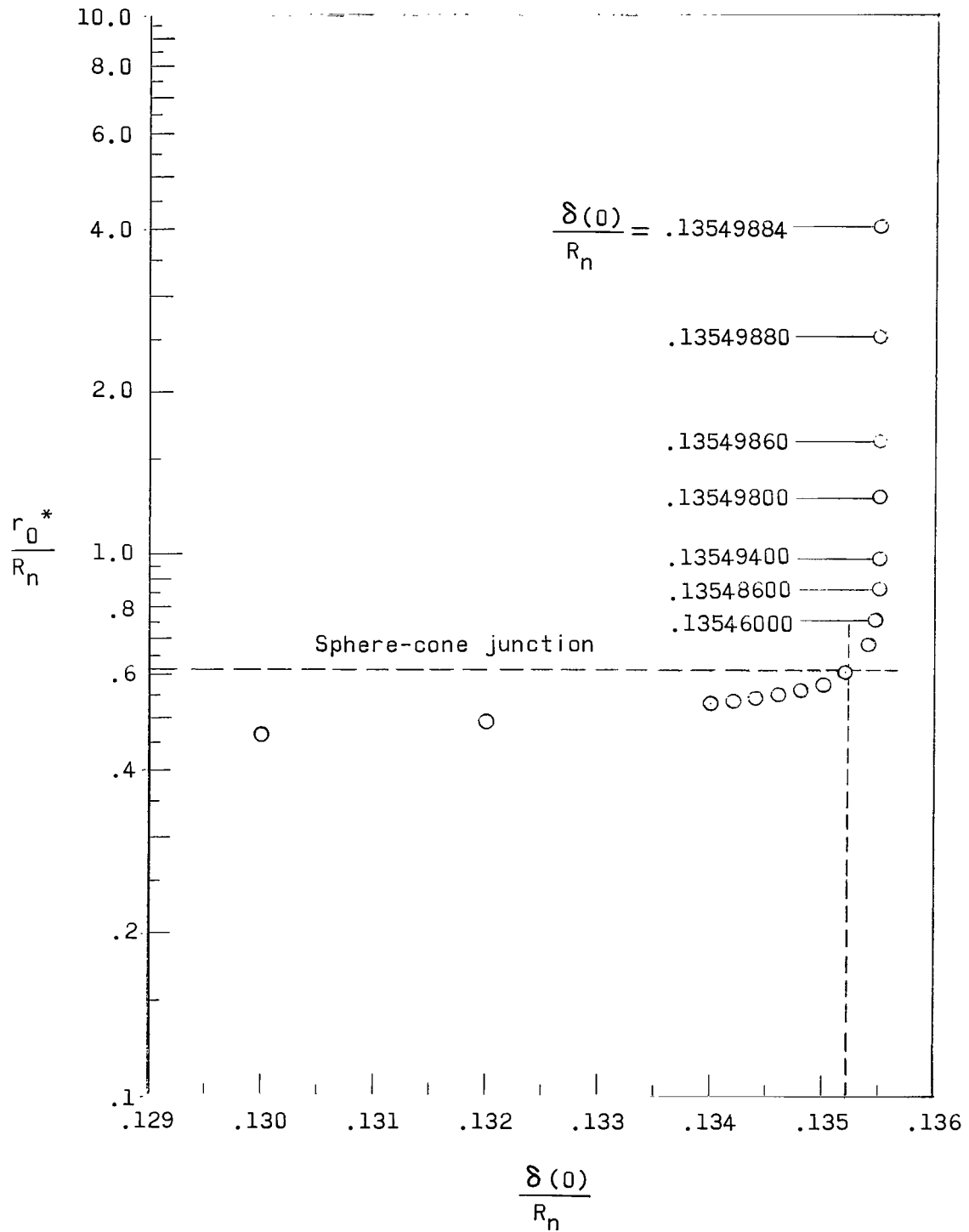


Figure 20.- Dependence of sonic singularity location on shock-wave standoff distance. $\gamma = 1.4$; $M_\infty = 10$; $\theta_c = 52^\circ$.

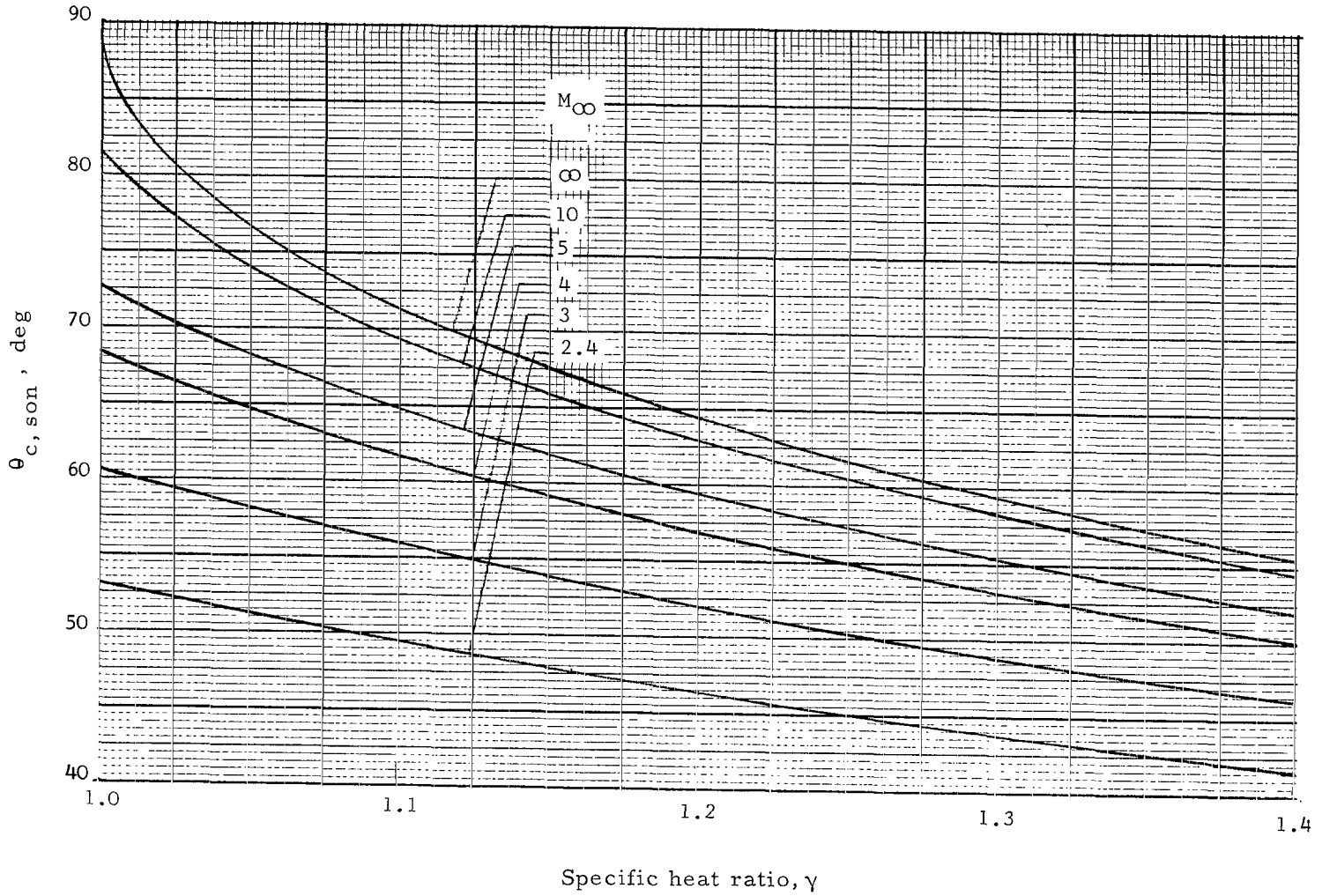


Figure 21.- Chart of sonic condition for pointed cone.



NATIONAL AERONAUTICS AND SPACE ADMINISTRATION
 WASHINGTON, D. C. 20546
 OFFICIAL BUSINESS

POSTAGE AND FEES PAID
 NATIONAL AERONAUTICS AND
 SPACE ADMINISTRATION

FIRST CLASS MAIL

02U 001 26 51 3DS 6
 AIR FORCE WEAPONS LABORATO
 KIRTLAND AIR FORCE BASE, N

ATT MISS MADELINE F. CANOV
 I TRADY /WIT /

POSTMASTER: If Undeliverable (Section 158
 Postal Manual) Do Not Return

"The aeronautical and space activities of the United States shall be conducted so as to contribute . . . to the expansion of human knowledge of phenomena in the atmosphere and space. The Administration shall provide for the widest practicable and appropriate dissemination of information concerning its activities and the results thereof."

— NATIONAL AERONAUTICS AND SPACE ACT OF 1958

NASA SCIENTIFIC AND TECHNICAL PUBLICATIONS

TECHNICAL REPORTS: Scientific and technical information considered important, complete, and a lasting contribution to existing knowledge.

TECHNICAL NOTES: Information less broad in scope but nevertheless of importance as a contribution to existing knowledge.

TECHNICAL MEMORANDUMS: Information receiving limited distribution because of preliminary data, security classification, or other reasons.

CONTRACTOR REPORTS: Scientific and technical information generated under a NASA contract or grant and considered an important contribution to existing knowledge.

TECHNICAL TRANSLATIONS: Information published in a foreign language considered to merit NASA distribution in English.

SPECIAL PUBLICATIONS: Information derived from or of value to NASA activities. Publications include conference proceedings, monographs, data compilations, handbooks, sourcebooks, and special bibliographies.

TECHNOLOGY UTILIZATION PUBLICATIONS: Information on technology used by NASA that may be of particular interest in commercial and other non-aerospace applications. Publications include Tech Briefs, Technology Utilization Reports and Notes, and Technology Surveys.

Details on the availability of these publications may be obtained from:

SCIENTIFIC AND TECHNICAL INFORMATION DIVISION
 NATIONAL AERONAUTICS AND SPACE ADMINISTRATION
 Washington, D.C. 20546